© 2019. Published by The Company of Biologists Ltd | Journal of Cell Science (2019) 132, jcs224766. doi:10.1242/jcs.224766

RESEARCH ARTICLE

Peroxisomes control mitochondrial dynamics and the mitochondrion-dependent apoptosis pathway

Hideaki Tanaka[1], Tomohiko Okazaki[1,*], Saeko Aoyama[1], Mutsumi Yokota[2], Masato Koike[2], Yasushi Okada[3,4], Yukio Fujiki[5] and Yukiko Gotoh[1]

ABSTRACT

Peroxisomes cooperate with mitochondria in the performance of cellular metabolic functions, such as fatty acid oxidation and the maintenance of redox homeostasis. However, whether peroxisomes also regulate mitochondrial fission–fusion dynamics or mitochondrion-dependent apoptosis remained unclear. We now show that genetic ablation of the peroxins Pex3 or Pex5, which are essential for peroxisome biogenesis, results in mitochondrial fragmentation in mouse embryonic fibroblasts (MEFs) in a manner dependent on Drp1 (also known as DNM1L). Conversely, treatment with 4-PBA, which results in peroxisome proliferation, resulted in mitochondrial elongation in wild-type MEFs, but not in Pex3-knockout MEFs. We further found that peroxisome deficiency increased the levels of cytosolic cytochrome *c* and caspase activity under basal conditions without inducing apoptosis. It also greatly enhanced etoposide-induced caspase activation and apoptosis, which is indicative of an enhanced cellular sensitivity to death signals. Taken together, our data unveil a previously unrecognized role for peroxisomes in the regulation of mitochondrial dynamics and mitochondrion-dependent apoptosis. Effects of peroxin gene mutations on mitochondrion-dependent apoptosis may contribute to pathogenesis of peroxisome biogenesis disorders.

This article has an associated First Person interview with the first author of the paper.

KEY WORDS: Drp1, Apoptosis, Caspase, Mitochondria, Organelle, Peroxisome

INTRODUCTION

Peroxisomes are organelles bound by a single membrane that play essential roles in metabolic functions such as oxidation of fatty acid chains, catabolism of reactive oxygen species (ROS), and synthesis of ether phospholipids in all eukaryotic cells. The peroxin (Pex) family of proteins is required for the assembly and function of peroxisomes (Waterham and Ebberink, 2012; Fujiki et al., 2012). Deficiency of Pex3, a peroxisomal membrane protein necessary for membrane assembly, thus results in the complete loss of peroxisomes (Muntau et al., 2000), whereas deficiency of Pex5, a peroxisomal transporter, results in the loss of peroxisomal matrix proteins (Otera et al., 1998). Peroxisomal dysfunction due to *Pex* gene mutations is detrimental to human development, as evidenced by human autosomal recessive genetic diseases (known as peroxisome biogenesis disorders), such as Zellweger syndrome, which results in death within the first year of life (Goldfischer et al., 1973). Peroxisome-deficient mice also die during the neonatal period (Maxwell et al., 2003; Baes et al., 1997). Both patients with peroxisome biogenesis disorders and peroxisome-deficient mice manifest a variety of characteristics including neurological dysfunction, hypotonia and craniofacial abnormalities (Trompier et al., 2014; Waterham and Ebberink, 2012; Muntau et al., 2000).

Peroxisomes collaborate with other organelles in various physiological and pathological contexts. In particular, peroxisomes engage in a functional interplay with mitochondria with regard to the degradation of fatty acids and ROS detoxification as well as to antiviral immunity (Lismont et al., 2015; Schrader and Yoon, 2007; Dixit et al., 2010). The interplay between peroxisomes and mitochondria is highlighted by the observation that the loss of *Pex* genes gives rise to abnormalities in mitochondrial structure and metabolic function. For instance, deletion of *Pex5* in mouse hepatocytes affects the structure of mitochondrial inner and outer membranes as well as giving rise to abnormal (swollen) cristae (Goldfischer et al., 1973; Peeters et al., 2015; Baumgart et al., 2001), reduced activity of oxidative phosphorylation (OXPHOS) complexes, loss of the mitochondrial membrane potential and increased ROS levels (Peeters et al., 2015). Deletion of *Pex5* has also been shown to increase the number of mitochondria as well as the level of glycolytic activity, possibly as a compensatory response to the impairment of OXPHOS (Peeters et al., 2015). Deletion of *Pex13* in mouse brain or of *Pex19* in fly larvae resulted in similar dysfunction of OXPHOS, elevated ROS levels, and an increased abundance of mitochondria (Rahim et al., 2016; Bülow et al., 2018). Furthermore, human patients harboring *PEX16* mutations manifest myopathy accompanied by mitochondrial abnormalities (Salpietro et al., 2015). It remains unclear, however, which of these various phenotypes in mice, flies and humans reflect primary effects of peroxisome deficiency or are secondary to primary effects such as ROS accumulation.

In addition to their roles in OXPHOS and redox regulation, mitochondria are key players in the regulation of apoptosis. Various proteins that are normally localized to the intermembrane space of mitochondria, including cytochrome *c*, are released into the cytosol on apoptosis induction. In the cytosol, cytochrome *c* interacts with Apaf-1 and pro-caspase-9 to form a large protein complex known as the apoptosome. The resulting increase in the autocatalytic activity of pro-caspase-9 leads to the cleavage and activation of pro-caspase-3 and pro-caspase-7, and the active forms of these latter two enzymes then execute apoptosis by cleaving numerous substrates (Wang and Youle, 2009).

[1]Graduate School of Pharmaceutical Sciences, IRCN, The University of Tokyo, Tokyo 113-0033, Japan. [2]Department of Cell Biology and Neuroscience, Juntendo University School of Medicine, Tokyo 113-8421, Japan. [3]Laboratory for Cell Dynamics Observation, Center for Biosystems Dynamics Research (BDR), RIKEN, Osaka 565-0874, Japan. [4]Department of Physics, Universal Biology Institute (UBI), and the International Research Center for Neurointelligence (WPI-IRCN), The University of Tokyo, Tokyo 113-0033, Japan. [5]Division of Organelle Homeostasis, Medical Institute of Bioregulation, Kyushu University, Fukuoka 812-8582, Japan.

*Author for correspondence (tokazaki@mol.f.u-tokyo.ac.jp)

H.T., 0000-0003-0549-839X; T.O., 0000-0002-8616-6671; Y.O., 0000-0003-2601-3689

Received 3 September 2018; Accepted 1 May 2019

Journal of Cell Science (2019) 132, jcs224766. doi:10.1242/jcs.224766

Mitochondria are highly dynamic organelles that continually change their morphology by fission and fusion processes, which contributes to mitochondrial quality control and the induction of apoptosis (Detmer and Chan, 2007; Suen et al., 2008). Mitochondrial fission and fusion are mediated by evolutionarily conserved members of the dynamin family of proteins. Fission is thus mediated by cytosolic dynamins, such as dynamin-related protein 1 (Drp1; also known as DNM1L) and Dyn2 (also known as DNM2), whereas fusion is mediated by the membrane-anchored dynamins Mfn1 and Mfn2, and Opa1 in mammals (Detmer and Chan, 2007; Lee et al., 2016). The fission process mediated by Drp1 appears to play a central role in the induction of cytochrome *c* release and subsequent apoptosis in various physiological and pathological contexts (Westermann, 2010).

Recent studies have shown that interactions with other organelles contribute to the regulation of mitochondrial dynamics. Sites of contact between mitochondria with endoplasmic reticulum (ER) (known as mitochondrion-associated membranes, MAMs) play an important role in the regulation of mitochondrial fission (Friedman et al., 2011) and have been implicated in that of apoptosis (Prudent et al., 2015; Yang et al., 2018; Hoppins and Nunnari, 2012). Lysosomes also participate in the regulation of mitochondrial dynamics (Wong et al., 2018). Mitochondria and peroxisomes share key regulators for their fission including Drp1, and as well as its receptors Fis1 and Mff (Kobayashi et al., 2007; Camões et al., 2009; Delille et al., 2009; Schrader, 2006). However, whether peroxisomes also regulate mitochondrial dynamics and mitochondrion-mediated apoptosis has remained unclear.

Here, we investigated the role of peroxisomes in the regulation of mitochondrial dynamics, caspase activation and apoptosis by deleting *Pex3* or *Pex5* in mouse embryonic fibroblasts (MEFs) under conditions in which the cytosolic ROS levels do not increase substantially. We found that deletion of either *Pex3* or *Pex5* resulted in fragmentation of mitochondria, the appearance of cytochrome *c* in the cytosol, and an increase in the amounts of cleaved caspase-9 and caspase-3. Importantly, restoration of Pex3 or Pex5 expression in the corresponding knockout (KO) MEFs attenuated these effects. Furthermore, we found that ablation of Pex3 greatly enhanced the induction of apoptosis by the DNA-damaging agent etoposide. Our results thus suggest that peroxisomes regulate mitochondrial dynamics, caspase activity and cell death so as to reduce cellular sensitivity to damaging insults.

RESULTS

Induction of mitochondrial fragmentation upon *Pex3* deletion

To examine an acute effect of peroxisome deficiency, we took advantage of MEFs derived from *Pex3*$^{fl/fl}$;*Rosa-Cre-ER*^{T2} mice, which are homozygous for a floxed allele of *Pex3* and harbor a tamoxifen-inducible transgene for Cre recombinase (Fig. S1A). We immortalized these cells by introducing SV40 large T antigen and deleted *Pex3* by adding 4-hydroxytamoxifen. Immunoblot analysis detected Pex3 protein in control MEFs (not exposed to 4-hydroxytamoxifen) but not in Pex3 KO MEFs (Fig. S1B). Immunofluorescence analysis also detected almost no punctate signals for Pex14 or for EGFP tagged with peroxisome-targeting signal 1 (PTS1), the signaling peptide present in peroxisome matrix proteins, in the Pex3 KO MEFs (Fig. S1C), indicating the successful depletion of peroxisomes in these cells.

With the use of our Pex3 KO MEFs, we then set out to identify mitochondrial phenotypes of peroxisome deficiency that could be rescued by reintroduction of peroxisomes. We examined mitochondrial morphology by observing the intracellular distribution of Tom20, a mitochondrial outer membrane protein, and ATP synthase β, a mitochondrial inner membrane protein, and found that the extent of mitochondrial fragmentation was increased in Pex3 KO MEFs (Fig. 1A,B). Huygens-based quantification indicated that the size of mitochondria was significantly smaller in Pex3 KO MEFs than that in control MEFs (Fig. 1C,D). The length of mitochondria also became shorter in Pex3 KO MEFs compared to that in control MEFs (Fig. S2B–E). We then asked whether restoration of Pex3 expression in these Pex3 KO cells would rescue this mitochondrial phenotype. Infection of Pex3 KO MEFs with a retrovirus encoding Pex3 increased the abundance of Pex3 protein and induced the formation of peroxisomes (Fig. S1D,E). Importantly, this reintroduction of Pex3 resulted in elongation of mitochondria in the Pex3-deficient MEFs (Fig. 1E–H), indicating that Pex3 suppresses mitochondrial fragmentation in a reversible manner.

Induction of mitochondrial fragmentation by *Pex5* deletion

Given that the effect of *Pex3* deletion on mitochondrial morphology might have been the result of a Pex3-specific function unrelated to peroxisome formation, we examined whether deletion of a different Pex gene, *Pex5*, confered a similar phenotype. Deletion of *Pex5* would be expected to result in loss of peroxisomal matrix proteins but retention of the peroxisomal membrane, whereas that of *Pex3* results in the complete loss of peroxisomes. To disrupt *Pex5* in MEFs, we adopted the CRISPR-Cas9 system with a guide (g)RNA targeted to *Pex5* (Fig. S3A). We confirmed disruption of *Pex5* gene (Fig. S3B) as well as the loss of Pex5 protein (Fig. 2A) in the targeted cells. Examination of mitochondrial morphology revealed that the extent of mitochondrial fragmentation was increased in the Pex5 KO MEFs compared with control (wild-type, WT) MEFs (Fig. 2B,C). Furthermore, this phenotype of Pex5 deficiency was rescued by retrovirus-mediated restoration of Pex5 expression (Fig. 2D–F). These results thus support the notion that peroxisomal functions are involved in suppressing mitochondrial fragmentation.

Induction of mitochondrial elongation by a peroxisome proliferator

We next examined whether an increase (rather than a decrease) in the number of peroxisomes might also affect mitochondrial morphology. We thus exposed MEFs to 4-phenylbutyrate (4-PBA), an inducer of peroxisome proliferation. We confirmed that 4-PBA increased the abundance of peroxisomes, as detected by immunostaining of Pex14, in control MEFs (Fig. 3A; Fig. S4A,B). Furthermore, we found that 4-PBA induced mitochondrial elongation in these cells (Fig. 3A,C, D; Fig. S4C,D). We also quantified the total mitochondrial number and volume, and found that 4-PBA treatment reduced the number of mitochondria without inducing significant changes in their total volume (Fig. S4G,H). These results further support the idea that 4-PBA treatment accelerated the mitochondrial fusion process or suppressed the fission process. Importantly, however, 4-PBA did not induce mitochondrial elongation or suppress mitochondrial fragmentation in Pex3 KO MEFs (Fig. 3B,C,E; Fig. S4E,F), suggesting that the induction of mitochondrial elongation by 4-PBA requires peroxisomes. Taken together, these results indicate that peroxisome abundance correlates well with mitochondrial volume and length.

Alteration of mitochondrial morphology and collapse of their cristae by *Pex3* deletion

Given the mitochondrial fragmentation apparent in peroxisome-deficient cells, we next examined mitochondrial structure in more detail by electron microscopy (EM). Mitochondria were indeed

Journal of Cell Science (2019) 132, jcs224766. doi:10.1242/jcs.224766

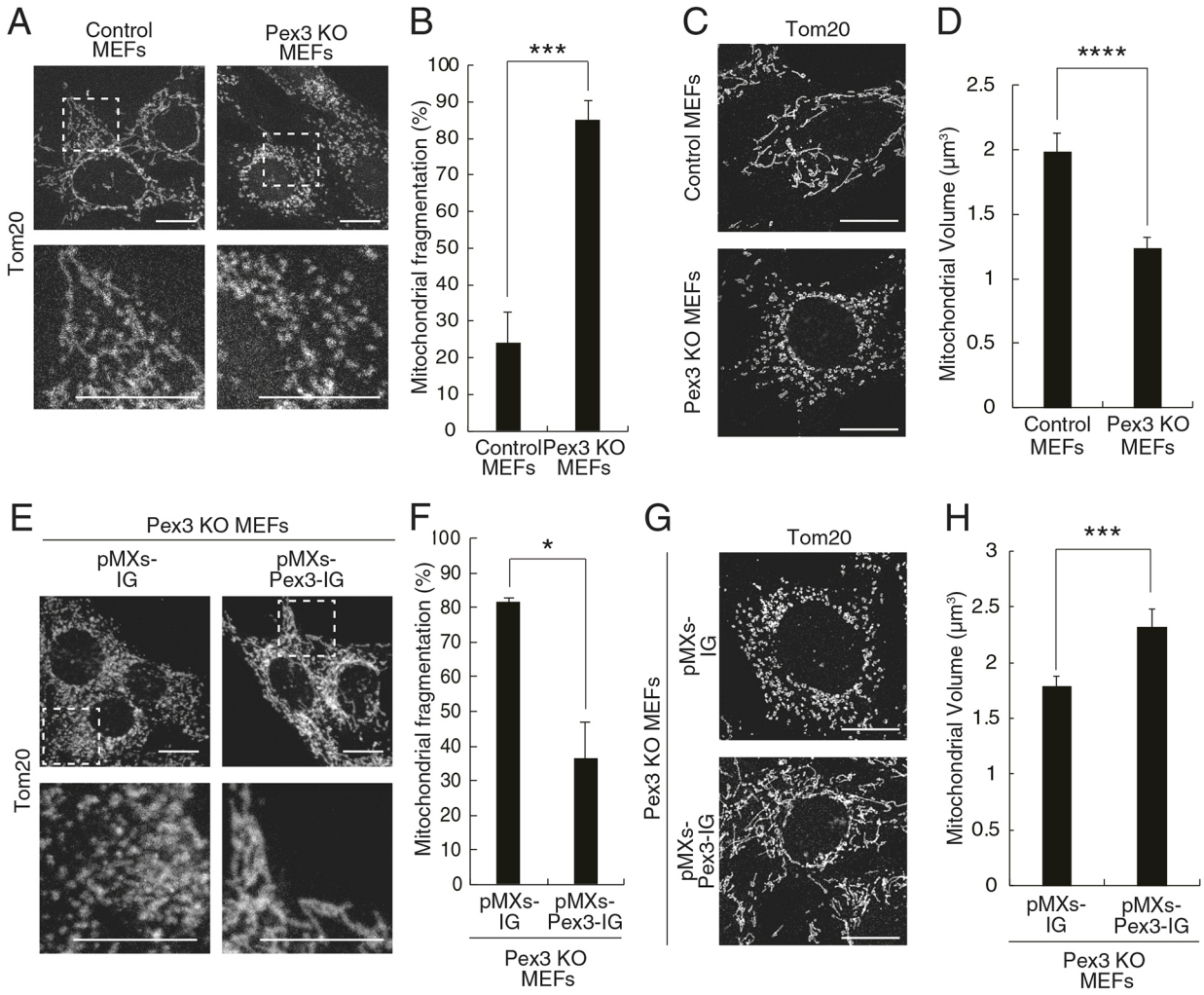

Fig. 1. Deletion of *Pex3* induces mitochondrial fragmentation. (A) Immunofluorescence staining of control and Pex3 KO MEFs with antibodies to Tom20. The boxed regions in the upper panels are shown at higher magnification in the lower panels. Scale bars: 20 µm. (B) Quantification of mitochondrial fragmentation (% of cells) in control and Pex3 KO MEFs determined from images as in A. Data are means±s.e.m. from three independent experiments. ***P<0.005 (unpaired Student's t-test). (C) Deconvolved immunofluorescence images of control and Pex3 KO MEFs with antibodies to Tom20. Scale bars: 20 µm. (D) Quantification of mitochondrial volume with the Huygens object analyzer as determined from images as in C. Data are means±s.e.m. from 35 cells in control MEFs and 30 cells in Pex3 KO MEFs from three independent experiments. Threshold, 15; Seed, 50. ****P<0.001 (unpaired Student's t-test). (E) Pex3 KO MEFs infected with retroviruses encoding GFP either alone (pMXs-IG) or together with Pex3 (pMXs-Pex3-IG) were subjected to immunofluorescence staining with antibodies to Tom20. The boxed regions in the upper panels are shown at higher magnification in the lower panels. Scale bars: 20 µm. (F) Quantification of mitochondrial fragmentation from images similar to those in E. Data are means±s.e.m. from three independent experiments. *P<0.05 (unpaired Student's t-test). (G) Deconvolved Immunofluorescence images of cells as in E with antibodies to Tom20. Scale bars: 20 µm. (H) Quantification of mitochondrial volume with the Huygens object analyzer as determined from images as in G. Data are means±s.e.m. from 60 cells in Pex3 KO MEFs infected with retroviruses encoding GFP, and 43 cells in Pex3 KO MEFs infected with retroviruses encoding GFP together with Pex3, and are from three independent experiments. Threshold, 30; Seed, 60. ***P<0.005 (unpaired Student's t-test).

smaller and shorter in Pex3 KO MEFs compared with control MEFs (Fig. 4A–C), consistent with the results of confocal fluorescence microscopy (Fig. 1A,B). The structure of cristae also appeared to have collapsed, with the presence of an indistinct and irregular inner membrane, in Pex3 KO MEFs (Fig. 4D), similar to the morphology previously observed in Pex5-deficient hepatocytes (Peeters et al., 2015; Baumgart et al., 2001).

Induction of cytochrome *c* diffusion by deletion of *Pex3*

Given that mitochondrial fragmentation and collapsed cristae are associated with the release of cytochrome *c* from these organelles and the intrinsic (mitochondrion-dependent) pathway of apoptosis (Suen et al., 2008; Otera et al., 2016), we examined whether *Pex3* deletion affected the distribution of cytochrome *c*. Whereas cytochrome *c* immunoreactivity was detected almost exclusively in mitochondria in control MEFs, as shown by its overlap with that of Tom20, cytochrome *c* signals were diffusely distributed in the cytosol in addition to their punctate mitochondrial distribution in Pex3 KO MEFs (Fig. 5A,B). A high cell density appeared to further increase the amount of cytochrome *c* in the cytosol of Pex3 KO cells (Fig. S5A). Quantitative analysis revealed that the colocalization of cytochrome *c* with Tom20, as reflected by Pearson's correlation coefficient (r), was significantly reduced in Pex3 KO MEFs compared with control MEFs (Fig. 5C), indicating that *Pex3* deletion indeed induced the diffusion of cytochrome *c*. Furthermore, subcellular fractionation analysis showed an increased ratio of cytosolic to mitochondrial cytochrome *c* in Pex3 KO MEFs as compared with control MEFs (Fig. 5D,E). This result further

Journal of Cell Science (2019) 132, jcs224766. doi:10.1242/jcs.224766

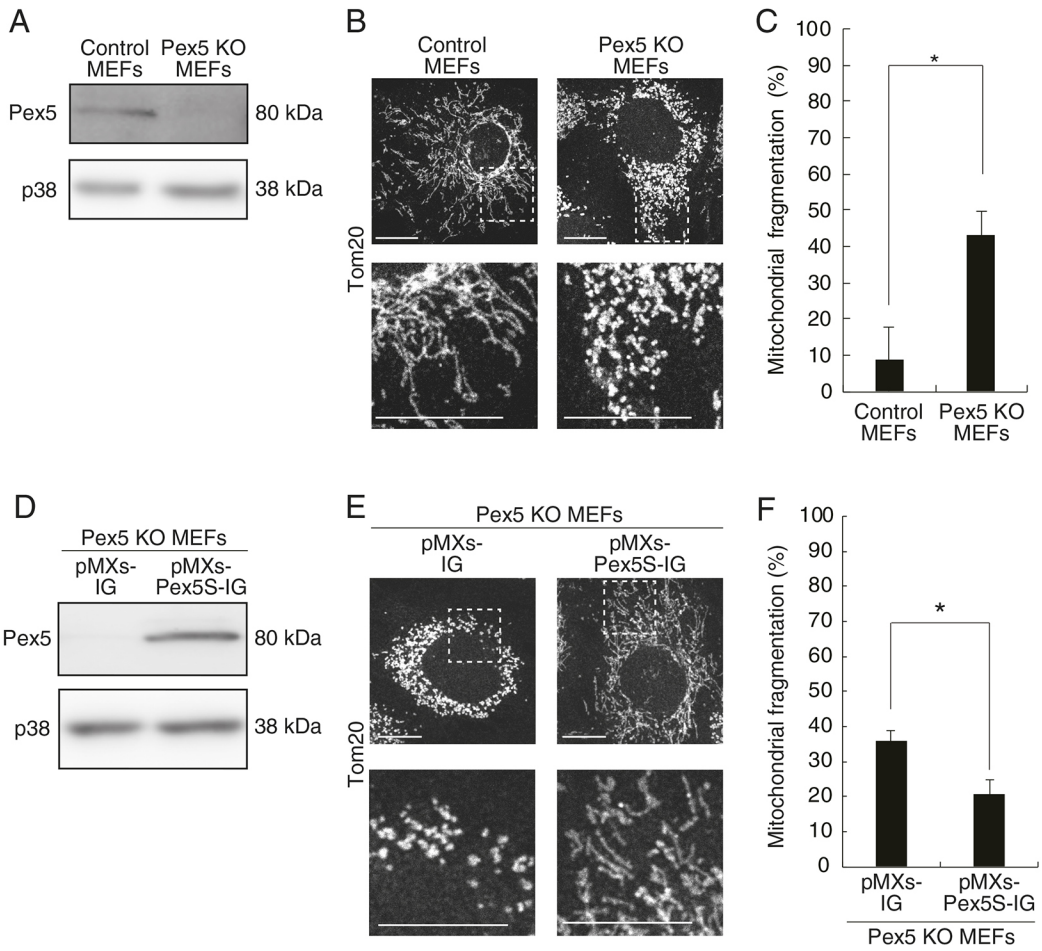

Fig. 2. Deletion of *Pex5* induces mitochondrial fragmentation. (A) Immunoblot analysis of Pex5 in control and Pex5 KO MEFs. Data are representative of three independent experiments. (B) Immunofluorescence analysis of Tom20 in control and Pex5 KO MEFs. The boxed regions in the upper panels are shown at higher magnification in the lower panels. Scale bars: 20 µm. (C) Quantification of mitochondrial fragmentation (% of cells) in control and Pex5 KO MEFs determined from images as in B. Data are means±s.e.m. from three independent experiments. **P*<0.05 (unpaired Student's *t*-test). (D) Immunoblot analysis of Pex5 in Pex5 KO MEFs infected with retroviruses encoding GFP either alone (pMXs-IG) or together with Pex5S (pMXs-Pex5S-IG). Data are representative of three independent experiments. (E) Immunofluorescence analysis of Tom20 in cells as in D. The boxed regions in the upper panels are shown at higher magnification in the lower panels. Scale bars: 20 µm. (F) Quantification of mitochondrial fragmentation in control and Pex5 KO MEFs determined from images as in E. Data are means±s.e.m. from four independent experiments. **P*<0.05 (unpaired Student's *t*-test).

confirms the diffusion of cytochrome *c* to the cytoplasm in Pex3 KO MEFs. Importantly, forced expression of Pex3 was sufficient to restore the normal (mitochondrial) distribution of cytochrome *c* in Pex3 KO MEFs (Fig. 5F–H). Together, these results thus show that Pex3 suppresses the diffusion of cytochrome *c*.

Induction of cytochrome *c* diffusion by deletion of *Pex5*

We then examined whether deletion of *Pex5* results in a similar redistribution of cytochrome *c*. Cytochrome *c* signals were indeed found to be diffusely distributed in the cytosol of Pex5 KO MEFs (Fig. 6A,B). We also confirmed that forced expression of Pex5 restored the mitochondrial localization of cytochrome *c* in the Pex5 KO cells (Fig. 6C,D). Together, our results thus indicate that functional peroxisomes, which require both Pex3 and Pex5, are necessary for suppression of cytochrome *c* diffusion.

Pex3 deletion does not cause an overt change in ROS and respiration levels

We next addressed the mechanism by which the diffusion of cytochrome *c* is increased in peroxisome-deficient MEFs. Although previous studies have shown that long-term deletion of *Pex* genes results in ROS accumulation (Bülow et al., 2018; Rahim et al., 2016), the cytosolic ROS level of our Pex3 KO MEFs as measured with a CellROX assay kit did not appear to differ from that of control MEFs (Fig. S6A,B). Under the same conditions, the treatment of these MEFs with tert-butylhydroperoxide (TBHP), a ROS inducer, increased CellROX signals (Fig. S6A,B). Moreover, control and Pex3 KO MEFs did not show a detectable difference in mitochondrial ROS levels as monitored by using MitoSOX (Fig. S6C,D). These results suggest that (relatively acute) *Pex3* deletion did not overtly increase ROS levels in mitochondria or the cytosol of our cultured MEFs. We also examined the rate of oxygen consumption in these cells, given that the abundance and activity of OXPHOS components are reduced after the deletion of *Pex* genes (Peeters et al., 2015). We again found, however, that control and Pex3 KO MEFs did not differ significantly in their basal or ATP-linked rates of oxygen consumption (Fig. S6E,F), suggesting that the mitochondrial OXPHOS system remains intact after *Pex3* deletion in MEFs. Considering that we did not observe overt ROS accumulation or altered oxygen consumption in these cells, it was

Journal of Cell Science (2019) 132, jcs224766. doi:10.1242/jcs.224766

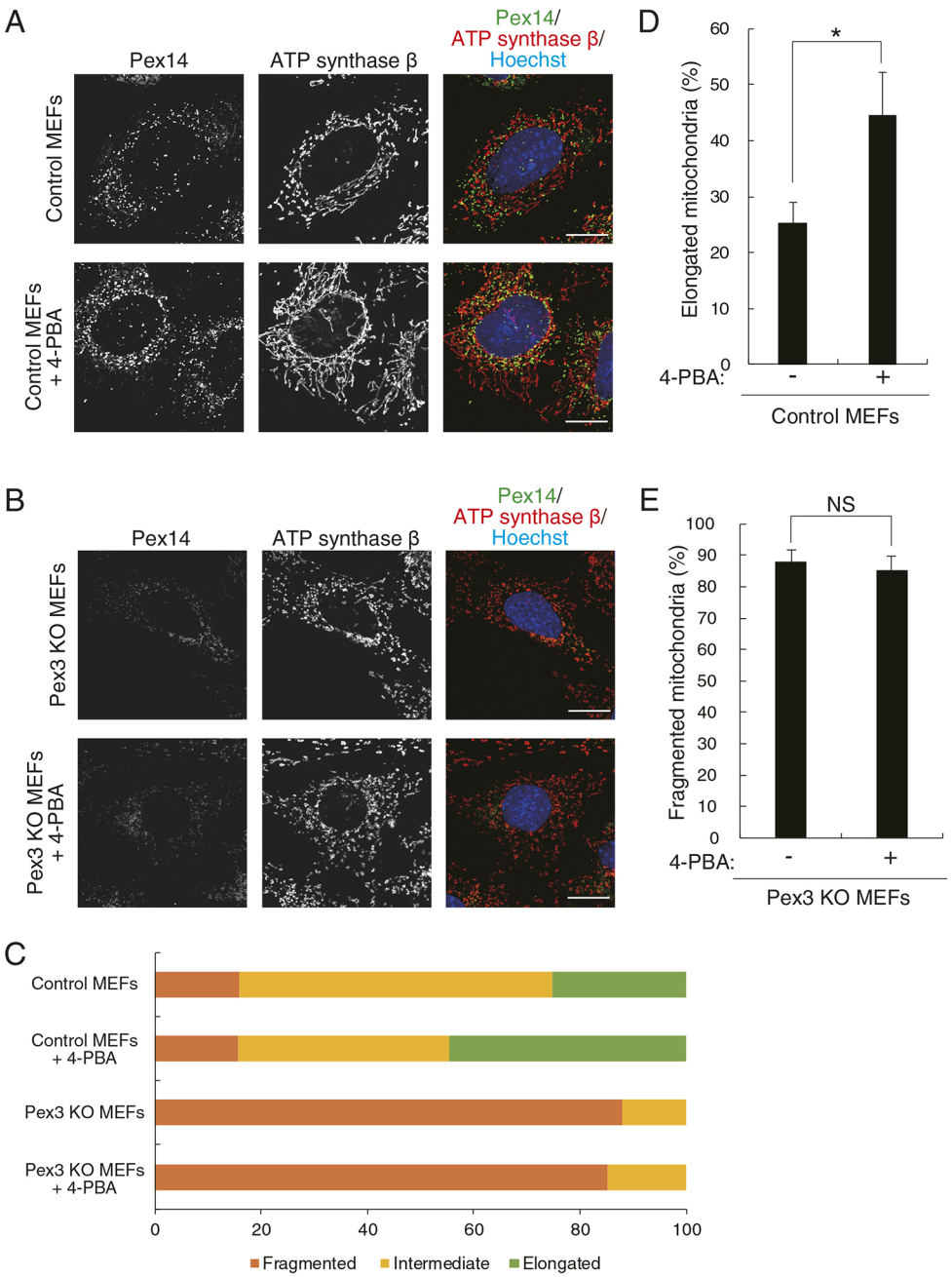

Fig. 3. The peroxisome proliferator 4-PBA induces mitochondrial elongation. (A) Immunofluorescence staining of Pex14 and ATP synthase β (a mitochondrial marker) in control MEFs cultured with or without 1 mM 4-PBA for 48 h. Nuclei were stained with Hoechst 33342 (1:10,000). Scale bars: 20 µm. (B) Immunofluorescence analysis of Pex3 KO MEFs cultured and stained as in A. Note that Pex14 signals that overlap with mitochondria in Pex3-deficient cells have been observed previously (Sugiura et al., 2017). (C) Summary of the quantification of mitochondrial morphology in control and Pex3 KO MEFs cultured with or without 1 mM 4-PBA for 48 h. (D) Quantification of mitochondrial elongation in control MEFs as in A. Data are means±s.e.m. for four independent experiments. **P*<0.05 (unpaired Student's *t*-test). (E) Quantification of mitochondrial fragmentation (% of cells) in Pex3 KO MEFs as in B. Data are means±s.e.m. for four independent experiments. NS, not significant (unpaired Student's *t*-test).

unlikely that an increase in ROS levels was responsible for the induction of cytochrome *c* diffusion. Indeed, treatment of Pex3 KO MEFs with the ROS scavenger *N*-acetylcysteine (NAC) did not suppress mitochondrial fragmentation or cytochrome *c* diffusion, whereas such treatment did attenuate the TBHP-induced increase in CellROX signal intensity (Fig. S6G–J).

Promotion of Drp1 association with mitochondria by deletion of *Pex3*

Given that Drp1 plays a pivotal role in mitochondrial fragmentation (fission) and cytochrome *c* release (Estaquier and Arnoult, 2007; Otera et al., 2016), and that Drp1 localizes not only to mitochondria but also to peroxisomes (Tanaka et al., 2006; Waterham et al., 2007), we examined whether *Pex3* deletion affects the abundance or subcellular localization of Drp1. Immunofluorescence analysis showed that the amounts of Drp1 both in the cytosol and associated with mitochondria appeared to increase in Pex3 KO MEFs compared with control MEFs (Fig. 7A). A western blot analysis also showed that the total amount of Drp1 proteins was increased upon Pex3 KO (Fig. S7A,B). Importantly, the extent of colocalization of Drp1, as well as that of its receptor Mff, with mitochondria was significantly higher in Pex3 KO MEFs than in control cells both in immunofluorescence and subcellular fractionation analyses (Fig. 7B–D; Fig. S7E–I), indicating that Pex3 ablation results in an increased localization of Drp1 to mitochondria, possibly through increasing the amount of Mff at mitochondria.

To examine whether Drp1 is responsible for the mitochondrial fragmentation and cytochrome *c* diffusion observed in Pex3 KO MEFs, we suppressed the function of Drp1 by introducing a catalytically inactive mutant (K38A) of the protein that has been shown to act in a dominant-negative manner (Frank et al., 2001). Expression of Drp1(K38A) indeed both restored the elongated

Journal of Cell Science (2019) 132, jcs224766. doi:10.1242/jcs.224766

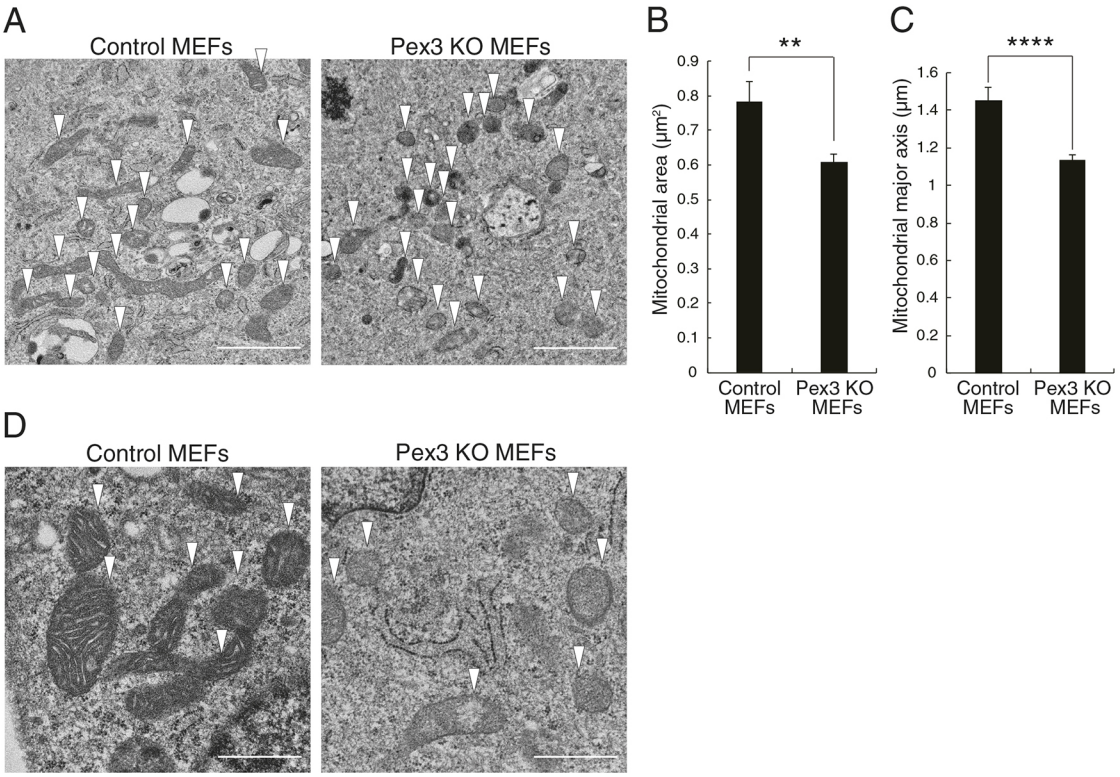

Fig. 4. Deletion of *Pex3* induces the collapse of mitochondrial cristae and their fragmentation. (A) Electron micrographs from control and Pex3 KO MEFs. Scale bars: 1 µm. (B,C) Quantification of mitochondrial area and length of the major axis, respectively, from images similar to those in A. Data are means±s.e.m. for 21 cells of each genotype. ***P*<0.01; *****P*<0.001 (unpaired Student's *t*-test). (D) High-magnification electron micrographs of control and Pex3 KO MEFs. Scale bars: 250 nm. Mitochondria are highlighted by arrowheads in A and D.

morphology of mitochondria and attenuated cytochrome *c* diffusion in Pex3 KO MEFs (Fig. 7E–G). In addition, siRNA-mediated knockdown of Drp1 rescued the morphological alterations of mitochondria in Pex3 KO MEFs (Fig. S7E,F). Together, these results thus suggested that *Pex3* deletion induces mitochondrial fragmentation and cytochrome *c* diffusion by promoting the localization of Drp1 to mitochondria.

Caspase activation and enhanced stress-induced apoptosis in Pex3 KO cells

The release of cytochrome *c* from mitochondria triggers activation of the Apaf-1–caspase-9 complex (apoptosome) and caspase-3 and thereby induces apoptosis (Hyman and Yuan, 2012). We therefore examined the effect of *Pex3* deletion on caspase activity and found that the levels of the cleaved forms of caspase-9 and caspase-3 were increased in Pex3 KO MEFs compared with control MEFs (Fig. 8A,B). These results thus suggested that Pex3 suppresses the activation of caspase-9 and caspase-3 under basal conditions in MEFs. In contrast, we did not detect any significant difference in the fraction of annexin V–positive (apoptotic) cells between control and Pex3 KO MEFs (Fig. 8C,D), suggesting that caspase activation induced by *Pex3* deletion is not sufficient to trigger apoptosis.

We hypothesized that the elevated basal activity of caspase-9 and caspase-3 in Pex3 KO MEFs might increase the vulnerability of these cells to cellular stressors that can trigger mitochondria-dependent apoptosis. To test this, we treated peroxisome-deficient cells with the DNA-damaging agent etoposide, a well-established inducer of mitochondria-dependent apoptosis (Yang et al., 1997; Wei et al., 2001; Karpinich et al., 2002). Both Pex3 KO MEFs and Pex5 KO MEFs manifested increased levels of caspase-3 activation in response to etoposide treatment compared with the corresponding control MEFs (Fig. 8E,F). Furthermore, annexin V staining revealed that Pex3 KO MEFs underwent apoptosis to a significantly greater extent than did control MEFs in response to etoposide treatment (Fig. 8G,H). Re-expression of Pex3 in Pex3 KO MEFs significantly suppressed the cellular apoptosis induced in response to etoposide (Fig. 8I), demonstrating that the phenotype was ascribable to Pex3 deletion. These results thus suggest that peroxisomes prevent excessive caspase activity and the induction of apoptosis, and that they thereby increase the resistance of cells to cellular stress such as that associated with DNA damage.

DISCUSSION

Although the cooperation between peroxisomes and mitochondria with regard to cellular metabolism has been extensively studied, the possible contribution of peroxisomes to mitochondrial fission–fusion dynamics has remained largely unknown. Our results now show that peroxisomes play a key role in determination of the balance between mitochondrial fission and fusion, with this balance being essential for a wide range of biological processes including cellular responsiveness to stressors (Khacho et al., 2016; Weir et al., 2017; Detmer and Chan, 2007). Indeed, our data also show that peroxisomes are important for protection of cells from mitochondrion-dependent apoptosis in response to DNA damage. Our study therefore provides a new basis for understanding the function of peroxisomes.

We found that the loss of peroxisomes induces the fragmentation of mitochondria in MEFs (Figs 1A–D, 2B,C, 4A–C; Fig. S2), whereas some studies have shown that the loss of peroxisomes in mouse serotogenic neurons and *Drosophila* Malpighian tubules instead

Journal of Cell Science (2019) 132, jcs224766. doi:10.1242/jcs.224766

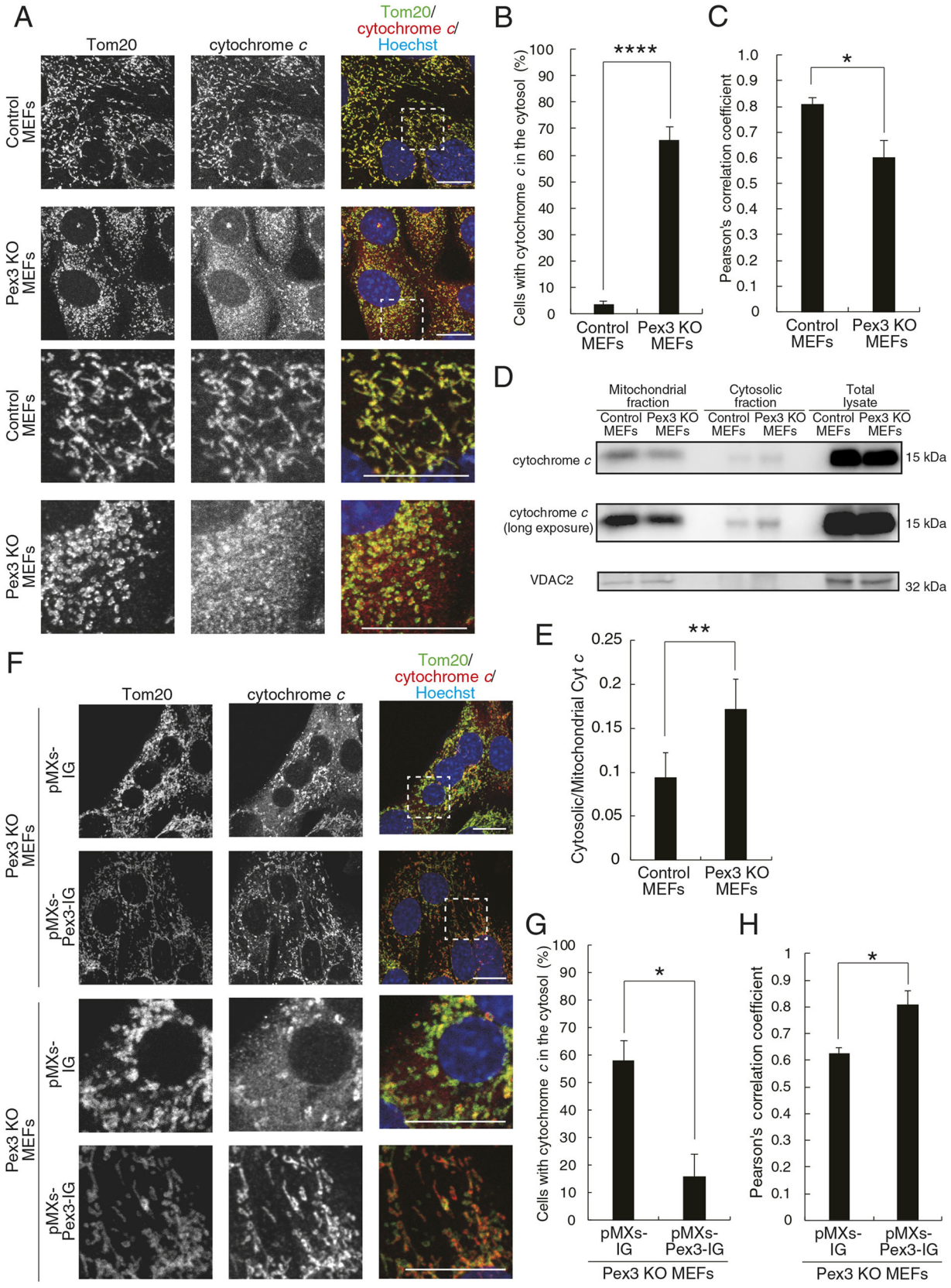

Fig. 5. See next page for legend.

resulted in the enlargement of mitochondria (Rahim et al., 2016; Bülow et al., 2018). Furthermore, a recent study has reported that human patient-derived fibroblasts lacking Pex3 did not exhibit changes in mitochondrial morphology (Sugiura et al., 2017). In addition to at the level of cells, tissues and species, these differences might be attributable to the long-term ablation of peroxins in these

Journal of Cell Science (2019) 132, jcs224766. doi:10.1242/jcs.224766

Fig. 5. Deletion of *Pex3* induces cytochrome *c* diffusion.
(A) Immunofluorescence staining of Tom20 and cytochrome *c* in control and Pex3 KO MEFs. The boxed regions in the upper panels are shown at higher magnification in the lower panels. Nuclei were stained with Hoechst 33342 (1:10,000). Scale bars: 20 µm. (B) Quantification of the cells with cytochrome *c* in the cytosol imaged as in A. Data are means±s.e.m. from three independent experiments. ****P<0.001 (unpaired Student's *t*-test). (C) Colocalization of cytochrome *c* with Tom20 as reflected by Pearson's correlation coefficient (*r*) and determined from images as in A. Data are means±s.e.m. from three independent experiments. *P<0.05 (unpaired Student's *t*-test). (D) Subcellular fractionation analysis of cytochrome *c* in control and Pex3 KO MEFs. Data are representative of three independent experiments. (E) Quantification of the cytosolic:mitochondrial cytochrome *c* (Cyt *c*) ratio from blots similar to those in D. Data are means±s.e.m. from three independent experiments. **P<0.01 (paired Student's *t*-test). (F) Immunofluorescence staining of Tom20 and cytochrome *c* in Pex3 KO MEFs infected with retroviruses encoding GFP either alone (pMXs-IG) or together with Pex3 (pMXs-Pex3-IG). The boxed regions in the upper panels are shown at higher magnification in the lower panels. Nuclei were stained with Hoechst 33342 (1:10,000). Scale bars: 20 µm. (G) Quantification of the proportion of cells with cytochrome *c* in the cytosol imaged as in F. Data are means±s.e.m. from three independent experiments. *P<0.05 (unpaired Student's *t*-test). (H) Colocalization of cytochrome *c* with Tom20 as reflected by Pearson's correlation coefficient and determined from images as in F. Data are means±s.e.m. from three independent experiments. *P<0.05 (unpaired Student's *t*-test).

studies, which likely resulted in secondary effects due to the accumulation of ROS and subsequent cellular damages. In this study, we took advantage of a MEF culture in which the intracellular ROS level was not significantly increased after peroxin ablation and found that the mitochondrial fragmentation and cytochrome *c* diffusion induced by peroxin gene deletion were rescued by restoration of peroxin expression, indicating that these phenomena are the primary effects of peroxisomal loss (Figs 1E–H, 2E,F, 5F–H, 6C,D).

The mechanism responsible for peroxisome-mediated regulation of mitochondrial fission–fusion dynamics remains unknown. Given that the fission machineries of both organelles share components such as Drp1, Fis1 and Mff in mammalian cells (Waterham et al., 2007; Tanaka et al., 2006; Schrader et al., 2012), peroxisomes and mitochondria may compete for these components. Indeed, we found that *Pex3* deletion increased localization of Drp1 and its receptor Mff to mitochondria (Fig. 7A–E, Fig. S7E–I), suggesting that the absence of peroxisomes promotes the recruitment of Drp1 to mitochondria by increasing the amount of its receptor at mitochondria. Furthermore, the inhibition of Drp1 rescued mitochondrial fragmentation in Pex3 KO MEFs (Fig. 7E–G; Fig. S7I,J). These results thus imply that Drp1 function is involved in the peroxisome-mediated regulation of mitochondrial dynamics. Several studies have also shown that peroxisomes are located adjacent to MAMs, which are described as mitochondrial constriction sites (Cohen et al., 2014; Mattiazzi Ušaj et al., 2015; Friedman et al., 2011; Horner et al., 2011). Given that peroxisomes also make physical contact with mitochondria (Fransen et al., 2017), these observations raise the possibility that peroxisomes compete with the ER for mitochondrial contact sites. Whether peroxisomes actually regulate MAM formation warrants future study. Furthermore, a recent study has shown that lysosomes also make contacts with mitochondria and regulate mitochondrial fission (Wong et al., 2018). Indeed, >80% of mitochondrial fission sites were found to contact lysosomes, whereas <20% of such sites contacted peroxisomes. Peroxisome–mitochondrion contacts may thus hamper or promote the interaction between lysosomes and mitochondria, resulting in modulation of the mitochondrial fission process. Together, these previous and present observations reveal multiple types of interorganellar communication that coordinately regulate mitochondrial fission–fusion dynamics.

Intriguingly, we noticed that the deletion of Pex5 affected mitochondrial morphology less dramatically than the deletion of Pex3. Furthermore, 4-PBA treatment slightly induced mitochondrial elongation in Pex5 KO MEFs as well as causing a slight increase in the number of peroxisomes (Fig. S8A,B). These results suggest that peroxisomal membranes or membrane proteins, which are retained in Pex5 KO MEFs but not in Pex3 KO MEFs, play a role in regulating mitochondrial morphology in addition to peroxisomal matrix proteins.

Given the findings in this study, we propose that Drp1 mediates mitochondrial fragmentation and subsequent cytochrome *c* diffusion in peroxisome-deficient cells. However, it remains unknown what molecular mechanism underlies cytochrome *c* diffusion after Drp1-mediated mitochondrial fragmentation in peroxisome-deficient cells. One possibility is that peroxisomes compete with mitochondria for some components necessary for cytochrome *c* diffusion. Cytochrome *c* is known to be released through the pore composed of the Bcl-2 family members Bax and Bak1 at the outer membrane of mitochondria (Tait and Green, 2010). In line with this, we checked the mitochondrial localization of Bax in Pex3 KO MEFs and found that the amounts of mitochondrial and cytosolic Bax in Pex3 KO MEFs were comparable to those in control MEFs (Fig. S5B,C). This result indicates that mitochondrial localization of Bax is not substantially affected by Pex3 deletion. Intriguingly, Fujiki and colleagues have reported that a fraction of Bak1 also localizes to peroxisomes (Hosoi et al., 2017). Elimination of peroxisomes may thus alter localization of Bak1 from peroxisomes to mitochondria, and the increased mitochondrial Bak1 may thereby facilitate cytochrome *c* diffusion in peroxisome-deficient cells. It would be important to test the notion that molecules shared by mitochondria and peroxisomes mediate their interorganellar communications.

Our results revealed not only the fragmentation of mitochondria in response to the loss of peroxisomes, but also the elongation of mitochondria in response to treatment of cells with an inducer of peroxisome proliferation, 4-PBA (Fig. 3; Fig. S4). These findings suggest that peroxisomal abundance is an important determinant of mitochondrial dynamics. Cellular conditions that affect the abundance of peroxisomes might thus also influence mitochondrial dynamics through peroxisomes. In this regard, cellular stressors such as UV light exposure and elevated ROS levels increase the number of peroxisomes in both plant and mammalian cells (Schrader and Fahimi, 2006). This increase in peroxisomal number or abundance may thus contribute to a protective response to allow cells to cope with stress via suppression of mitochondrial fragmentation and caspase activation. Such a notion is consistent with our present results showing that peroxisomes reduce cellular sensitivity to toxic insults.

Fatty acids, such as oleic acid, and a high-fat diet are also thought to increase the abundance of peroxisomes (Reddy and Mannaerts, 1994; Ishii et al., 1980; Diano et al., 2011; Lock et al., 1989; Veenhuis et al., 1987). It would thus be of interest to determine whether the high level of fatty acid synthesis apparent in adult neural stem-progenitor cells (Knobloch et al., 2013) confers resistance to cellular stress through an increase in the number of peroxisomes. Indeed, the abundance of peroxisomes is known to be high in radial glia cells preserved for a long period and to be reduced by aging (Ahlemeyer et al., 2007), with such changes possibly having consequences for mitochondrial regulation in these cells.

Mitochondrion-dependent activation of caspases contributes not only to removal of unnecessary cells during development or damaged cells exposed to stress stimuli but also to regulation of tissue stem cell differentiation and terminal differentiation of

Journal of Cell Science (2019) 132, jcs224766. doi:10.1242/jcs.224766

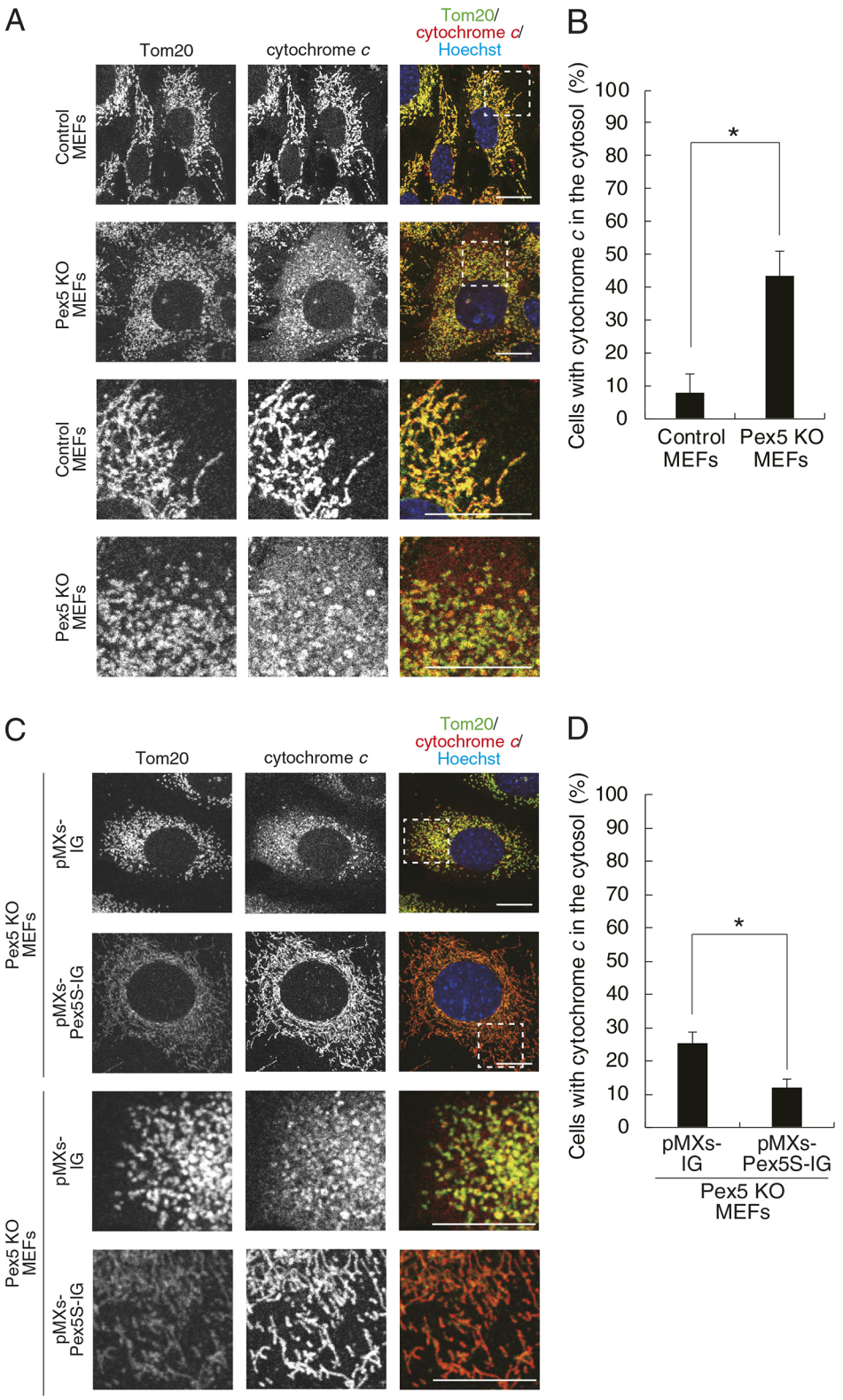

Fig. 6. Deletion of *Pex5* induces cytochrome *c* diffusion. (A) Immunofluorescence staining of Tom20 and cytochrome *c* in control and Pex5 KO MEFs. Nuclei were stained with Hoechst 33342 (1:10,000). The boxed regions in the upper panels are shown at higher magnification in the lower panels. Scale bars: 20 µm. (B) Quantification of the cells with cytochrome *c* in the cytosol imaged as in A. Data are means±s.e.m. from three independent experiments. **P*<0.05 (unpaired Student's *t*-test). (C) Immunofluorescence staining of Tom20 and cytochrome *c* in Pex5 KO MEFs infected with retroviruses encoding GFP either alone (pMXs-IG) or together with Pex5S (pMXs-Pex5S-IG). Nuclei were stained with Hoechst 33342 (1:10,000). The boxed regions in the upper panels are shown at higher magnification in the lower panels. Scale bars: 20 µm. (D) Quantification of the proportion of cells with cytochrome *c* in the cytosol imaged as in C. Data are means±s.e.m. from four independent experiments. **P*<0.05 (unpaired Student's *t*-test).

myoblasts, erythroblasts and keratinocytes (Hollville and Deshmukh, 2017). Furthermore, non-apoptotic caspase activation plays a key regulatory role in the pruning of neurites and the formation and maturation of neural circuits in the nervous system (Unsain and Barker, 2015). For example, caspase-9 is necessary for axon pruning in dorsal root ganglion neurons and cervical sympathetic neurons (Simon et al., 2012; Cusack et al., 2013). Non-apoptotic caspase activation is also implicated in regulation of the internalization of AMPA-sensitive glutamate receptors, which contributes to long-term depression in hippocampal neurons (Li et al., 2010). Non-apoptotic activation of caspases is thus essential for the control of various cellular processes. The activation of caspases at a sublethal level in peroxisome-deficient cells observed in the present study suggests that peroxisomes limit

Journal of Cell Science (2019) 132, jcs224766. doi:10.1242/jcs.224766

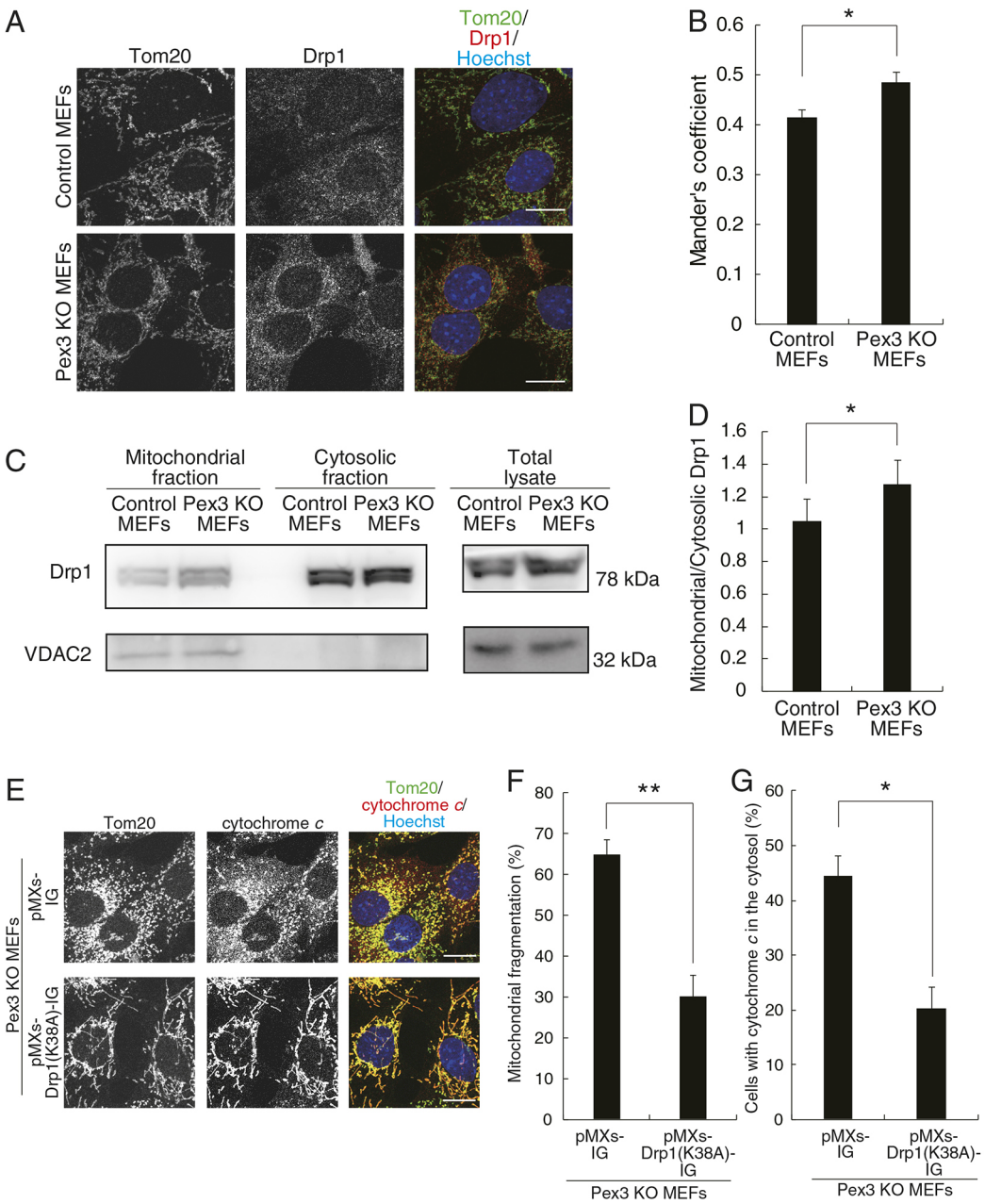

Fig. 7. Deletion of *Pex3* promotes the association of Drp1 with mitochondria. (A) Immunofluorescence staining of Tom20 and Drp1 in control and Pex3 KO MEFs. Nuclei were stained with Hoechst 33342 (1:10,000). Scale bars: 20 µm. (B) Colocalization of Drp1 with Tom20 as reflected by the Manders' M1 coefficient and determined from images as in A. Data are means±s.e.m. from five independent experiments. **P*<0.05 (unpaired Student's *t*-test). (C) Subcellular fractionation analysis of Drp1 in control and Pex3 KO MEFs. Data are representative of four independent experiments. (D) Quantification of the mitochondrial:cytosolic Drp1 ratio from blots similar to those in C. Data are means±s.e.m. from four independent experiments. **P*<0.05 (paired Student's *t*-test). (E) Immunofluorescence staining of Tom20 and cytochrome *c* in Pex3 KO MEFs infected with retroviruses encoding GFP either alone (pMXs-IG) or together with mutated Drp1 [Drp1(K38A)-IG]. Nuclei were stained with Hoechst 33342 (1:10,000). Scale bars: 20 µm. Data are representative of three independent experiments. (F) Quantification of mitochondrial fragmentation (% of cells) in images similar to those in E. Data are means±s.e.m. from three independent experiments. ***P*<0.01 (unpaired Student's *t*-test). (G) Quantification of the proportion of cells with cytochrome *c* in the cytosol imaged as in E. Data are means±s.e.m. from three independent experiments. **P*<0.05 (unpaired Student's *t*-test).

caspase activation under low-stress conditions (Fig. 8). It will be of interest to examine the possible role of peroxisomes in various biological processes that require non-apoptotic caspase activation.

Individuals with Zellweger syndrome and peroxin-deficient mice manifest severe defects in various organs including the brain, bone, muscle, kidney and liver. The mechanisms underlying this broad range of abnormalities, however, remain unknown. Dysfunction of the mitochondrial fusion machinery also gives rise to neurodegenerative diseases, muscle atrophy and osteogenic abnormalities (Detmer and Chan, 2007; Chen et al., 2010; Romanello et al., 2010; Touvier et al., 2015). Degeneration of Purkinje cells, one of the most prominent features of patients with Zellweger syndrome (Barry and O'Keeffe, 2013; Trompier et al., 2014), is thus also observed in mice with Purkinje cell-specific

Journal of Cell Science (2019) 132, jcs224766. doi:10.1242/jcs.224766

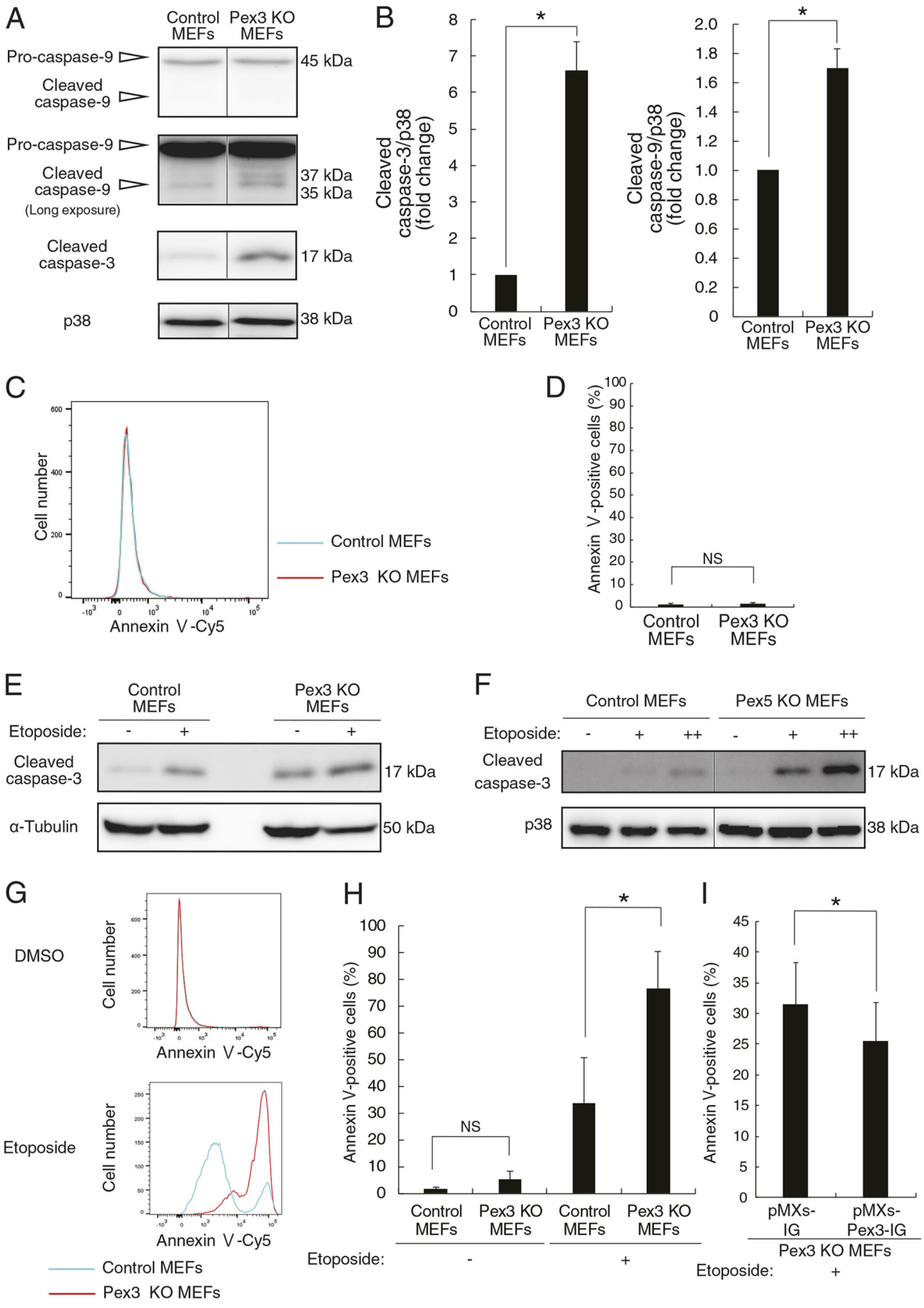

Fig. 8. See next page for legend.

deficiency of Mfn2 (Chen et al., 2007). The peroxisome-dependent regulation of mitochondria uncovered in the present study therefore raises the possibility that excessive mitochondrial fragmentation plays a causal role in the pathogenesis of Zellweger syndrome. If so, our findings may provide a basis for the development of new therapies for this lethal disease.

Fig. 8. Deletion of *Pex3* induces caspase activation and enhances stress-induced apoptosis. (A) Immunoblot analysis of caspase-3 and caspase-9 in control and Pex3 KO MEFs. The pro- and cleaved forms of the enzymes are indicated. Black vertical lines indicate noncontiguous lanes. (B) Quantification of the cleaved forms of caspase-3 and caspase-9 (normalized to the levels of p38 MAPK) in blots similar to those in A. Data are means±s.e.m. from three independent experiments. **P*<0.05 (paired Student's *t*-test). (C) Representative flow cytometric analysis of Cy5-labeled annexin V staining for control and Pex3 KO MEFs. (D) Quantification of cells positive for annexin V–Cy5 staining as in C. Data are means±s.e.m. from four independent experiments. NS, not significant (paired Student's *t*-test). (E,F) Immunoblot analysis of the cleaved form of caspase-3 in control and either Pex3 KO (E) or Pex5 KO (F) MEFs that had been incubated in the absence (–) or presence of etoposide at 2 (+) or 4 (++) µM for 24 h. Either α-tubulin or p38 MAPK was examined as a loading control. Black vertical lines indicate noncontiguous lanes. Data are representative of three independent experiments. (G) Representative flow cytometric analysis of annexin V–Cy5 staining for control and Pex3 KO MEFs that had been incubated for 24 h with 2 µM etoposide or DMSO vehicle. (H) Quantification of cells positive for annexin V–Cy5 staining as in G. Data are means±s.e.m. from three independent experiments. **P*<0.05; NS, not significant (Scheffe's test). (I) Quantification of cells positive for annexin V–Cy5 staining for Pex3 KO MEFs infected with retroviruses encoding GFP either alone (pMXs-IG) or together with Pex3 (pMXs-Pex3-IG) that had been incubated for 24 h with 2 µM etoposide. Data are means±s.e.m. from three independent experiments. **P*<0.05 (paired Student's *t*-test).

MATERIALS AND METHODS

Immunoblot analysis

Immunoblot analysis was performed as described previously (Okazaki et al., 2013). Immune complexes were detected with a chemiluminescence reagent (100 mM Tris-HCl pH 8.5, 1.25 mM luminol, 0.2 mM coumaric acid, 0.009% H_2O_2) and an Image Quant LAS4000 instrument (GE Healthcare). Blot intensities were measured with Image J software. In Figs 5D, 7C and Fig. S5B, subcellular fractionation analysis was performed by using a mitochondria/cytosol fractionation kit (K256-25; Biovision, Milpitas, CA,) according to the manufacturer's instructions. See 'Antibodies' section below for details of antibodies used.

Immunofluorescence microscopy

Cells were fixed with 4% formaldehyde for 10 min at 37°C, permeabilized with 0.2% Triton X-100 in PBS for 5 min, and incubated for 30 min in PBS containing 2% fetal bovine serum (FBS) and 2% bovine serum albumin (BSA) (blocking buffer). They were then exposed first for 24 h at 4°C to primary antibodies in blocking buffer and then for 1 h at room temperature to Alexa Fluor-conjugated secondary antibodies (Thermo Fisher Scientific) and Hoechst 33342 in blocking buffer. Moviol were used as mounting medium. Images were acquired with a TCS SP5 confocal microscope (Leica) and were processed with Photoshop CS software (Adobe). For cytochrome *c* staining, only secondary antibodies were utilized for immunofluorescence in order to check the specificity of these signals. The Pearson's correlation coefficient (*r*) for the colocalization of Tom20 and cytochrome *c* as well as the Manders' M1 coefficient for the colocalization of Tom20 and Drp1 were calculated with Coloc 2 of Fiji. See 'Antibodies' section below for details of antibodies used.

Morphological quantification of mitochondria

In Fig. 1A,B,E,F, Fig. 2B,C,E,F, Fig. 3A–E, Fig. 7E,F, Fig. S6H,I, mitochondria were labeled by antibodies against Tom20 or ATP synthase β. Mitochondrial morphology of individual cells was evaluated in a double-blinded analysis and classified into 'fragmented mitochondria', 'intermediate mitochondria' and 'elongated mitochondria' (see Fig. S2A).

In Fig. 1C,D,G,H and Fig. 4A–H, samples were prepared in the same way as in the immunofluorescence experiments, except that ProLong Diamond (Thermo Fisher Scientific) were used as mounting medium. We took the 3D images in order to match the Nyquist condition (pixel size of *x* and *y*, 50 nm; *z*, 100 nm). These images were deconvoluted in Huygens software (Scientific Volume Imaging). After the deconvolution process, individual mitochondria were defined with the Huygens object analyzer. The values of seed and threshold were described in each figure legends. After the definition of mitochondria, their voxels and length of were calculated with object analyzer. Cellular average of mitochondrial volume and/or length were calculated in each condition.

Electron microscopy

Cells were fixed in 0.1 M phosphate buffer (pH 7.2) containing 2% glutaraldehyde and 2% paraformaldehyde, exposed to 1% OsO_4, dehydrated, and embedded in Epon 812. Ultrathin sections (60 nm) were cut with an ultramicrotome (UC6, Leica Microsystems), stained with uranyl acetate and lead citrate, and examined with a Hitachi HT7700 electron microscope. The area and major axis of mitochondria in images were measured with the use of Fiji software.

Measurement of ROS

Cells were incubated with 5 µM MitoSOX or 500 nM CellROX for 30 min at 37°C, isolated by exposure to trypsin, and resuspended in PBS containing 3% FBS for analysis with a FACSAria flow cytometer (BD Biosciences).

Measurement of oxygen consumption rate

The oxygen consumption rate (OCR) of cells was measured with the use of a Seahorse XF24 Extracellular Flux Analyzer (Seahorse Biosciences). Cells were plated in 24-well Seahorse plates and cultured overnight, after which the medium was replaced with Seahorse XF Base medium supplemented with 10 mM glucose, 1 mM pyruvate and GlutaMAX (2 ml/liter, Thermo Fisher Scientific). The cells were placed in a 37°C incubator without CO_2 before loading into the analyzer. After measurement of basal respiration, the cells were exposed to 1 µM oligomycin to measure the proton leak, to 1 µM carbonylcyanide m-chlorophenylhydrazone (CCCP) to measure the maximal OCR, and to 0.5 µM rotenone and 0.5 µM antimycin A to measure the non-mitochondrial OCR. The ATP-linked OCR was calculated by subtracting the proton leak from basal OCR. Cells plated simultaneously in 96-well plates were counted to normalize OCR values.

Annexin V binding assay

Cells were stained with Cy5-coupled annexin V (Promokine) according to the manufacturer's instructions. Flow cytometric analysis of the stained cells was performed with a FACSAria flow cytometer (BD Biosciences).

Cell culture and transfection

MEFs and Plat-E cells (Morita et al., 2000) were maintained in Dulbecco's modified Eagle's medium (DMEM) supplemented with 10% FBS and 1% penicillin-streptomycin. Plat-E cells were transfected with the use of the GeneJuice Transfection Reagent (Merck Millipore), whereas transfection of MEFs was performed with Lipofectamine 2000 or with Lipofectamine and PLUS Reagents (Thermo Fisher Scientific).

Deletion of *Pex3*

C57BL/6 mice harboring the *Pex3*$^{tm3a(EUCOMM)Wtsi}$ allele obtained from the EUCOMM (European Conditional Mouse Mutagenesis Program) consortium were crossed with *Act-FLP* transgenic mice (Kono et al., 2017) to remove the FRT-flanked region and subsequently with *Rosa-CreER*^{T2} transgenic mice (obtained from the U.S. National Cancer Institute) (Fig. S1). Mice heterozygous for the floxed allele of *Pex3* were mated, and the resulting homozygous embryos were isolated for preparation of MEFs. All animal experiments were performed according to approved guidelines. The MEFs were immortalized by the introduction of SV40 large T antigen as described previously (Ando et al., 2000), and they were then treated with 1 nM 4-hydroxytamoxifen to remove the loxP-flanked region. Immortalized MEFs treated with ethanol vehicle instead of 4-hydroxytamoxifen were prepared as control cells.

Deletion of *Pex5*

3T3 MEFs (kindly provided by Hidenori Ichijo, Graduate School of Pharmaceutical Sciences, The University of Tokyo, Japan) were transfected with the KO vector (see 'Plasmids' section below) and were then sorted with

a FACSAria flow cytometer (BD Biosciences) to obtain GFP-positive cells, which were seeded as single cells in a 96-well plate.

Genomic PCR analysis

For confirmation of *Pex5* deletion in MEFs, the cells were collected and lysed with genotyping buffer [50 mM KCl, 10 mM Tris-HCl pH 8.3, 1.5 mM $MgCl_2$, 0.1 mg/ml gelatin, 0.45% NP-40, 0.45% Tween 20, proteinase K (500 µg/ml, Kanto Chemical)] or lysis buffer (1% SDS, 10 mM EDTA, 50 mM Tris-HCl pH 8.1) and were then incubated consecutively at 55°C for 3 h and 98°C for 10 min. The *Pex5* locus was amplified by PCR with the use of KOD FX Neo (Toyobo) and the forward and reverse primers 5′-TCCCT-TCCCCCAGCCCACTCCGGGTGCCTC-3′ and 5′-TCGGCGATGAATT-CTTGGGACCAGTCGGTCTCATT-3′. The PCR products were ligated into PCR-Blunt (Thermo Fisher Scientific) for sequencing by Eurofin Genomics.

Retrovirus-mediated expression of Pex3, Pex5 and Drp1(K38A)

Plat-E cells were transfected with pMXs-IG, or either pMXs-Pex3-IG vector encoding human Pex3 or pMXs-Pex5S-IG vectors encoding Chinese hamster Pex5S, or pMXs-Drp1(K38A)-IG vector encoding rat Drp1(K38A) (Morita et al., 2000). After 3 days, the culture supernatants were harvested for isolation of retroviruses. Pex3 KO or Pex5 KO MEFs were infected with the corresponding peroxin retrovirus or the control virus, after which the cells were sorted with a FACSAria flow cytometer (BD Biosciences) to obtain GFP-positive cells. For preparing Drp1(K38A)-infected cells, Pex3 KO MEFs were infected with the Drp1(K38A) retrovirus or the control virus and infected cells were sorted in the same way as above.

Plasmids

The plasmid pUcD2Hyg/EGFP-PTS1 was described previously (Tamura et al., 1998). Full-length cDNAs for human Pex3 or Chinese hamster Pex5S (His-ClPex5S-HA) (Ghaedi et al., 2000; Matsumura et al., 2000) were subcloned into the BamHI and XhoI sites of the pMXs-IG vector (kindly provided by Toshio Kitamura, Division of Cellular Therapy/Division of Stem Cell Signaling, The Institute of Medical Sciences, The University of Tokyo, Japan). The p3xFLAG-ratDrp1K38A plasmid encoding rat Drp1(K38A) was kindly provided by Naotada Ishihara, Department of Biological Sciences, Graduate School of Science, Osaka University, Japan. Full-length cDNAs for rat Drp1(K38A) were subcloned into the EcoRI and XhoI sites of the pMXs-IG vector. For generation of the CRISPR vector for *Pex5* deletion, a pair of oligonucleotides encoding the gRNA (forward, 5′-CACCGCTGGTCACCATGGCAATGC-3′; reverse, 5′-AAACGCATT-GCCATGGTGACCAGC-3′) was annealed and ligated into the px458 vector (Ran et al., 2013).

RNA interference

Silencer Select siRNAs (Thermo Fisher Scientific) were used for Drp1-knockdown experiments. Cells were transfected with siRNA oligonucleotides with the Lipofectamine RNAiMAX Reagent (Thermo Fisher Scientific). The cells were then used for subsequent assays after incubation for 72 h. The siRNA sequences were 5′-CGAUUGAAGGAACCGCAAATT-3′ and 5′-GCAAUUGAGCUAGCGUAUATT-3′. The negative control #1 and #2 siRNA [Thermo Fisher Scientific, catalog nos 4390843 (#1) and 4390847 (#2)] were used as controls.

Reagents

NAC was obtained from Sigma-Aldrich. Etoposide, Hoechst 33342, a CellROX Green Flow Cytometry Assay Kit (including TBHP, NAC), ProLong Diamond, and MitoSOX Red Reagents were obtained from Thermo Fisher Scientific. The Seahorse XF Cell Mito Stress Test Kit was obtained from Primetech. 4-PBA was obtained from Tocris.

Antibodies

Polyclonal and monoclonal antibodies to cleaved caspase-3 (#9661, #9664; 1:500) and to Mfn2 (#9482S; 1:500) were obtained from Cell Signaling; antibodies to p38 MAPK (sc-535; 1:1000), to Tom20 (sc-11415; 1:400) and to Bax (sc-493; 1:1000) were from Santa Cruz Biotechnology; those to α-tubulin (T6199; 1:1000) were from Sigma; those to cytochrome *c* [556432; 1:400 for immunofluorescence (IF), 556433; 1:500 for western blotting (WB)] and to Drp1 (611112; 1:400 for IF, 1:1000 for WB) were from BD Pharmingen; those to Pex14 (10594-1-AP; 1:400) and to Mff (17090-1-AP; 1:100 for IF, 1:500 for WB) were from Proteintech; those to Pex3 (HPA042830; 1:500) were from Atlas Antibodies; those to ATP synthase β (A21351; 1:400) were from Thermo Fisher Scientific; those to caspase-9 (M054-3; 1:500) were from MBL Life Science; those to Mfn1 (ab57602; 1:500) and to VDAC2 (ab47104; 1:500) were from Abcam; and those to Pex5 were described previously (Okumoto et al., 2014).

Statistical analysis

Quantitative data are presented as means±s.e.m. and were compared with Scheffe's test or the two-tailed unpaired or paired Student's *t*-test. A P value of <0.05 was considered statistically significant.

Acknowledgements

We thank M. Okajima (Graduate School of Pharmaceutical Sciences, The University of Tokyo) for technical assistance, N. Ishihara (Institute of Life Science, Kurume University) and T. Kitamura (The Institute of Medical Sciences, The University of Tokyo) for providing the plasmids, H. Ichijo (Graduate School of Pharmaceutical Sciences, The University of Tokyo) for providing the cells. We also appreciate our laboratory members for discussions.

Competing interests

The authors declare no competing or financial interests.

Author contributions

Conceptualization: H.T., T.O., Y.F., Y.G.; Methodology: H.T., M.Y., M.K., Y.O.; Software: Y.O.; Formal analysis: H.T., M.Y.; Investigation: H.T., S.A.; Resources: Y.F.; Data curation: H.T.; Writing - original draft: H.T.; Writing - review & editing: H.T., T.O., Y.F., Y.G.; Visualization: M.Y., M.K., Y.O.; Supervision: T.O., Y.G.; Project administration: H.T., T.O., Y.G.; Funding acquisition: T.O., Y.F., Y.G.

Funding

This work was supported by a Grant-in-Aid from the Ministry of Education, Culture, Sports, Science, and Technology (MEXT) of Japan; by the Core Research for Evolutionary Science and Technology of the Japan Science and Technology Agency; and in part by research fellowships from the Japan Society for the Promotion of Science (JSPS) and the Global Centers of Excellence Program (Integrative Life Science Based on the Study of Biosignaling Mechanisms) of MEXT; by the Graduate Program for Leaders in Life Innovation, The University of Tokyo Life Innovation Leading Graduate School, of MEXT; and by JSPS KAKENHI grants JP26116007, JP17H03675, JP16H05773, JP16H06280 and JP18J14098.

Supplementary information

Supplementary information available online at
http://jcs.biologists.org/lookup/doi/10.1242/jcs.224766.supplemental

References

Ahlemeyer, B., Neubert, I., Kovacs, W. J. and Baumgart-Vogt, E. (2007). Differential expression of peroxisomal matrix and membrane proteins during postnatal development of mouse brain. *J. Comp. Neurol.* **505**, 1-17. doi:10.1002/cne.21448

Ando, H., Kobayashi, M., Toda, S., Kikkawa, F., Masahashi, T. and Mizutani, S. (2000). Establishment of a ciliated epithelial cell line from human Fallopian tube. *Hum. Reprod.* **15**, 1597-1603. doi:10.1093/humrep/15.7.1597

Baes, M., Gressens, P., Baumgart, E., Carmeliet, P., Casteels, M., Fransen, M., Evrard, P., Fahimi, D., Declercq, P. E., Collen, D. et al. (1997). A mouse model for Zellweger syndrome. *Nat. Genet.* **17**, 49-57. doi:10.1038/ng0997-49

Barry, D. S. and O'Keeffe, G. W. (2013). Peroxisomes: the neuropathological consequences of peroxisomal dysfunction in the developing brain. *Int. J. Biochem. Cell Biol.* **45**, 2012-2015. doi:10.1016/j.biocel.2013.06.019

Baumgart, E., Vanhorebeek, I., Grabenbauer, M., Borgers, M., Declercq, P. E., Fahimi, H. D. and Baes, M. (2001). Mitochondrial alterations caused by defective peroxisomal biogenesis in a mouse model for Zellweger syndrome (PEX5 knockout mouse). *Am. J. Pathol.* **159**, 1477-1494. doi:10.1016/S0002-9440(10)62534-5

Bülow, M. H., Wingen, C., Senyilmaz, D., Gosejacob, D., Sociale, M., Bauer, R., Schulze, H., Sandhoff, K., Teleman, A. A., Hoch, M. et al. (2018). Unbalanced lipolysis results in lipotoxicity and mitochondrial damage in peroxisome-deficient. *Mol. Biol. Cell* **29**, 396-407. doi:10.1091/mbc.E17-08-0535

Camões, F., Bonekamp, N. A., Delille, H. K. and Schrader, M. (2009). Organelle dynamics and dysfunction: A closer link between peroxisomes and mitochondria. *J. Inherit. Metab. Dis.* **32**, 163-180. doi:10.1007/s10545-008-1018-3

Chen, H., McCaffery, J. M. and Chan, D. C. (2007). Mitochondrial fusion protects against neurodegeneration in the cerebellum. *Cell* **130**, 548-562. doi:10.1016/j.cell.2007.06.026

Chen, H., Vermulst, M., Wang, Y. E., Chomyn, A., Prolla, T. A., McCaffery, J. M. and Chan, D. C. (2010). Mitochondrial fusion is required for mtDNA stability in skeletal muscle and tolerance of mtDNA mutations. *Cell* **141**, 280-289. doi:10.1016/j.cell.2010.02.026

Cohen, Y., Klug, Y. A., Dimitrov, L., Erez, Z., Chuartzman, S. G., Elinger, D., Yofe, I., Soliman, K., Gärtner, J., Thoms, S. et al. (2014). Peroxisomes are juxtaposed to strategic sites on mitochondria. *Mol. Biosyst.* **10**, 1742-1748. doi:10.1039/C4MB00001C

Cusack, C. L., Swahari, V., Hampton Henley, W., Michael Ramsey, J. and Deshmukh, M. (2013). Distinct pathways mediate axon degeneration during apoptosis and axon-specific pruning. *Nat. Commun.* **4**, 1876. doi:10.1038/ncomms2910

Delille, H. K., Alves, R. and Schrader, M. (2009). Biogenesis of peroxisomes and mitochondria: linked by division. *Histochem. Cell Biol.* **131**, 441-446. doi:10.1007/s00418-009-0561-9

Detmer, S. A. and Chan, D. C. (2007). Functions and dysfunctions of mitochondrial dynamics. *Nat. Rev. Mol. Cell Biol.* **8**, 870-879. doi:10.1038/nrm2275

Diano, S., Liu, Z.-W., Jeong, J. K., Dietrich, M. O., Ruan, H.-B., Kim, E., Suyama, S., Kelly, K., Gyengesi, E., Arbiser, J. L. et al. (2011). Peroxisome proliferation-associated control of reactive oxygen species sets melanocortin tone and feeding in diet-induced obesity. *Nat. Med.* **17**, 1121-1127. doi:10.1038/nm.2421

Dixit, E., Boulant, S., Zhang, Y., Lee, A. S. Y., Odendall, C., Shum, B., Hacohen, N., Chen, Z. J., Whelan, S. P., Fransen, M. et al. (2010). Peroxisomes are signaling platforms for antiviral innate immunity. *Cell* **141**, 668-681. doi:10.1016/j.cell.2010.04.018

Estaquier, J. and Arnoult, D. (2007). Inhibiting Drp1-mediated mitochondrial fission selectively prevents the release of cytochrome c during apoptosis. *Cell Death Differ.* **14**, 1086-1094. doi:10.1038/sj.cdd.4402107

Frank, S., Gaume, B., Bergmann-Leitner, E. S., Leitner, W. W., Robert, E. G., Catez, F., Smith, C. L. and Youle, R. J. (2001). The role of dynamin-related protein 1, a mediator of mitochondrial fission, in apoptosis. *Dev. Cell* **1**, 515-525. doi:10.1016/S1534-5807(01)00055-7

Fransen, M., Lismont, C. and Walton, P. (2017). The peroxisome-mitochondria connection: how and why? *Int. J. Mol. Sci.* **18**, 1126. doi:10.3390/ijms18061126

Friedman, J. R., Lackner, L. L., West, M., DiBenedetto, J. R., Nunnari, J. and Voeltz, G. K. (2011). ER tubules mark sites of mitochondrial division. *Science* **334**, 358-362. doi:10.1126/science.1207385

Fujiki, Y., Yagita, Y. and Matsuzaki, T. (2012). Peroxisome biogenesis disorders: molecular basis for impaired peroxisomal membrane assembly: in metabolic functions and biogenesis of peroxisomes in health and disease. *Biochim. Biophys. Acta* **1822**, 1337-1342. doi:10.1016/j.bbadis.2012.06.004

Ghaedi, K., Tamura, S., Okumoto, K., Matsuzono, Y. and Fujiki, Y. (2000). The peroxin pex3p initiates membrane assembly in peroxisome biogenesis. *Mol. Biol. Cell* **11**, 2085-2102. doi:10.1091/mbc.11.6.2085

Goldfischer, S., Moore, C. L., Johnson, A. B., Spiro, A. J., Valsamis, M. P., Wisniewski, H. K., Ritch, R. H., Norton, W. T., Rapin, I. and Gartner, L. M. (1973). Peroxisomal and mitochondrial defects in the cerebro-hepato-renal syndrome. *Science* **182**, 62-64. doi:10.1126/science.182.4107.62

Hollville, E. and Deshmukh, M. (2017). Physiological functions of non-apoptotic caspase activity in the nervous system. *Semin. Cell Dev. Biol.* **82**, 127-136. doi:10.1016/j.semcdb.2017.11.037

Hoppins, S. and Nunnari, J. (2012). Mitochondrial dynamics and apoptosis–the ER connection. *Science* **337**, 1052-1054. doi:10.1126/science.1224709

Horner, S. M., Liu, H. M., Park, H. S., Briley, J. and Gale, M. (2011). Mitochondrial-associated endoplasmic reticulum membranes (MAM) form innate immune synapses and are targeted by hepatitis C virus. *Proc. Natl. Acad. Sci. USA* **108**, 14590-14595. doi:10.1073/pnas.1110133108

Hosoi, K.-I., Miyata, N., Mukai, S., Furuki, S., Okumoto, K., Cheng, E. H. and Fujiki, Y. (2017). The VDAC2-BAK axis regulates peroxisomal membrane permeability. *J. Cell Biol.* **216**, 709-722. doi:10.1083/jcb.201605002

Hyman, B. T. and Yuan, J. (2012). Apoptotic and non-apoptotic roles of caspases in neuronal physiology and pathophysiology. *Nat. Rev. Neurosci.* **13**, 395-406. doi:10.1038/nrn3228

Ishii, H., Fukumori, N., Horie, S. and Suga, T. (1980). Effects of fat content in the diet on hepatic peroxisomes of the rat. *Biochim. Biophys. Acta* **617**, 1-11. doi:10.1016/0005-2760(80)90218-0

Karpinich, N. O., Tafani, M., Rothman, R. J., Russo, M. A. and Farber, J. L. (2002). The course of etoposide-induced apoptosis from damage to DNA and p53 activation to mitochondrial release of cytochrome c. *J. Biol. Chem.* **277**, 16547-16552. doi:10.1074/jbc.M110629200

Khacho, M., Clark, A., Svoboda, D. S., Azzi, J., MacLaurin, J. G., Meghaizel, C., Sesaki, H., Lagace, D. C., Germain, M., Harper, M.-E. et al. (2016). Mitochondrial dynamics impacts stem cell identity and fate decisions by regulating a nuclear transcriptional program. *Cell Stem Cell* **19**, 232-247. doi:10.1016/j.stem.2016.04.015

Knobloch, M., Braun, S. M. G., Zurkirchen, L., von Schoultz, C., Zamboni, N., Araúzo-Bravo, M. J., Kovacs, W. J., Karalay, O., Suter, U., Machado, R. A. C. et al. (2013). Metabolic control of adult neural stem cell activity by Fasn-dependent lipogenesis. *Nature* **493**, 226-230. doi:10.1038/nature11689

Kobayashi, S., Tanaka, A. and Fujiki, Y. (2007). Fis1, DLP1, and Pex11p coordinately regulate peroxisome morphogenesis. *Exp. Cell Res.* **313**, 1675-1686. doi:10.1016/j.yexcr.2007.02.028

Kono, J., Konno, K., Talukder, A. H., Fuse, T., Abe, M., Uchida, K., Horio, S., Sakimura, K., Watanabe, M. and Itoi, K. (2017). Distribution of corticotropin-releasing factor neurons in the mouse brain: a study using corticotropin-releasing factor-modified yellow fluorescent protein knock-in mouse. *Brain Struct. Funct.* **222**, 1705-1732. doi:10.1007/s00429-016-1303-0

Lee, J. E., Westrate, L. M., Wu, H., Page, C. and Voeltz, G. K. (2016). Multiple dynamin family members collaborate to drive mitochondrial division. *Nature* **540**, 139-143. doi:10.1038/nature20555

Li, Z., Jo, J., Jia, J.-M., Lo, S.-C., Whitcomb, D. J., Jiao, S., Cho, K. and Sheng, M. (2010). Caspase-3 activation via mitochondria is required for long-term depression and AMPA receptor internalization. *Cell* **141**, 859-871. doi:10.1016/j.cell.2010.03.053

Lismont, C., Nordgren, M., Van Veldhoven, P. P. and Fransen, M. (2015). Redox interplay between mitochondria and peroxisomes. *Front. Cell Dev. Biol.* **3**, 35. doi:10.3389/fcell.2015.00035

Lock, E. A., Mitchell, A. M. and Elcombe, C. R. (1989). Biochemical mechanisms of induction of hepatic peroxisome proliferation. *Annu. Rev. Pharmacol. Toxicol.* **29**, 145-163. doi:10.1146/annurev.pa.29.040189.001045

Matsumura, T., Otera, H. and Fujiki, Y. (2000). Disruption of the interaction of the longer isoform of Pex5p, Pex5pL, with Pex7p abolishes peroxisome targeting signal type 2 protein import in mammals. Study with a novel Pex5-impaired Chinese hamster ovary cell mutant. *J. Biol. Chem.* **275**, 21715-21721. doi:10.1074/jbc.M000721200

Mattiazzi Ušaj, M., Brložnik, M., Kaferle, P., Žitnik, M., Wolinski, H., Leitner, F., Kohlwein, S. D., Zupan, B. and Petrovič, U. (2015). Genome-wide localization study of yeast Pex11 identifies peroxisome-mitochondria interactions through the ERMES complex. *J. Mol. Biol.* **427**, 2072-2087. doi:10.1016/j.jmb.2015.03.004

Maxwell, M., Bjorkman, J., Nguyen, T., Sharp, P., Finnie, J., Paterson, C., Tonks, I., Paton, B. C., Kay, G. F. and Crane, D. I. (2003). Pex13 inactivation in the mouse disrupts peroxisome biogenesis and leads to a Zellweger syndrome phenotype. *Mol. Cell. Biol.* **23**, 5947-5957. doi:10.1128/MCB.23.16.5947-5957.2003

Morita, S., Kojima, T. and Kitamura, T. (2000). Plat-E: an efficient and stable system for transient packaging of retroviruses. *Gene Ther.* **7**, 1063-1066. doi:10.1038/sj.gt.3301206

Muntau, A. C., Mayerhofer, P. U., Paton, B. C., Kammerer, S. and Roscher, A. A. (2000). Defective peroxisome membrane synthesis due to mutations in human PEX3 causes Zellweger syndrome, complementation group G. *Am. J. Hum. Genet.* **67**, 967-975. doi:10.1086/303071

Okazaki, T., Higuchi, M. and Gotoh, Y. (2013). Mitochondrial localization of the antiviral signaling adaptor IPS-1 is important for its induction of caspase activation. *Genes Cells* **18**, 493-501. doi:10.1111/gtc.12052

Okumoto, K., Noda, H. and Fujiki, Y. (2014). Distinct modes of ubiquitination of peroxisome-targeting signal type 1 (PTS1) receptor Pex5p regulate PTS1 protein import. *J. Biol. Chem.* **289**, 14089-14108. doi:10.1074/jbc.M113.527937

Otera, H., Okumoto, K., Tateishi, K., Ikoma, Y., Matsuda, E., Nishimura, M., Tsukamoto, T., Osumi, T., Ohashi, K., Higuchi, O. et al. (1998). Peroxisome targeting signal type 1 (PTS1) receptor is involved in import of both PTS1 and PTS2: studies with PEX5-defective CHO cell mutants. *Mol. Cell. Biol.* **18**, 388-399. doi:10.1128/MCB.18.1.388

Otera, H., Miyata, N., Kuge, O. and Mihara, K. (2016). Drp1-dependent mitochondrial fission via MiD49/51 is essential for apoptotic cristae remodeling. *J. Cell Biol.* **212**, 531-544. doi:10.1083/jcb.201508099

Peeters, A., Shinde, A. B., Dirkx, R., Smet, J., De Bock, K., Espeel, M., Vanhorebeek, I., Vanlander, A., Van Coster, R., Carmeliet, P. et al. (2015). Mitochondria in peroxisome-deficient hepatocytes exhibit impaired respiration, depleted DNA, and PGC-1α independent proliferation. *Biochim. Biophys. Acta* **1853**, 285-298. doi:10.1016/j.bbamcr.2014.11.017

Prudent, J., Zunino, R., Sugiura, A., Mattie, S., Shore, G. C. and McBride, H. M. (2015). MAPL SUMOylation of Drp1 stabilizes an ER/mitochondrial platform required for cell death. *Mol. Cell* **59**, 941-955. doi:10.1016/j.molcel.2015.08.001

Rahim, R. S., Chen, M., Nourse, C. C., Meedeniya, A. C. B. and Crane, D. I. (2016). Mitochondrial changes and oxidative stress in a mouse model of Zellweger syndrome neuropathogenesis. *Neuroscience* **334**, 201-213. doi:10.1016/j.neuroscience.2016.08.001

Ran, F. A., Hsu, P. D., Wright, J., Agarwala, V., Scott, D. A. and Zhang, F. (2013). Genome engineering using the CRISPR-Cas9 system. *Nat. Protoc.* **8**, 2281-2308. doi:10.1038/nprot.2013.143

Reddy, J. K. and Mannaerts, G. P. (1994). Peroxisomal lipid metabolism. *Annu. Rev. Nutr.* **14**, 343-370. doi:10.1146/annurev.nu.14.070194.002015

Romanello, V., Guadagnin, E., Gomes, L., Roder, I., Sandri, C., Petersen, Y., Milan, G., Masiero, E., Del Piccolo, P., Foretz, M. et al. (2010). Mitochondrial fission and remodelling contributes to muscle atrophy. *EMBO J.* **29**, 1774-1785. doi:10.1038/emboj.2010.60

Salpietro, V., Phadke, R., Saggar, A., Hargreaves, I. P., Yates, R., Fokoloros, C., Mankad, K., Hertecant, J., Ruggieri, M., McCormick, D. et al. (2015). Zellweger syndrome and secondary mitochondrial myopathy. *Eur. J. Pediatr.* **174**, 557-563. doi:10.1007/s00431-014-2431-2

Schrader, M. (2006). Shared components of mitochondrial and peroxisomal division. *Biochim. Biophys. Acta* **1763**, 531-541. doi:10.1016/j.bbamcr.2006.01.004

Schrader, M. and Fahimi, H. D. (2006). Peroxisomes and oxidative stress. *Biochim. Biophys. Acta* **1763**, 1755-1766. doi:10.1016/j.bbamcr.2006.09.006

Schrader, M. and Yoon, Y. (2007). Mitochondria and peroxisomes: are the 'big brother' and the 'little sister' closer than assumed? *BioEssays* **29**, 1105-1114. doi:10.1002/bies.20659

Schrader, M., Bonekamp, N. A. and Islinger, M. (2012). Fission and proliferation of peroxisomes. *Biochim. Biophys. Acta* **1822**, 1343-1357. doi:10.1016/j.bbadis.2011.12.014

Simon, D. J., Weimer, R. M., McLaughlin, T., Kallop, D., Stanger, K., Yang, J., O'Leary, D. D. M., Hannoush, R. N. and Tessier-Lavigne, M. (2012). A caspase cascade regulating developmental axon degeneration. *J. Neurosci.* **32**, 17540-17553. doi:10.1523/JNEUROSCI.3012-12.2012

Suen, D.-F., Norris, K. L. and Youle, R. J. (2008). Mitochondrial dynamics and apoptosis. *Genes Dev.* **22**, 1577-1590. doi:10.1101/gad.1658508

Sugiura, A., Mattie, S., Prudent, J. and McBride, H. M. (2017). Newly born peroxisomes are a hybrid of mitochondrial and ER-derived pre-peroxisomes. *Nature* **542**, 251-254. doi:10.1038/nature21375

Tait, S. W. G. and Green, D. R. (2010). Mitochondria and cell death: outer membrane permeabilization and beyond. *Nat. Rev. Mol. Cell Biol.* **11**, 621-632. doi:10.1038/nrm2952

Tamura, S., Okumoto, K., Toyama, R., Shimozawa, N., Tsukamoto, T., Suzuki, Y., Osumi, T., Kondo, N. and Fujiki, Y. (1998). Human PEX1 cloned by functional complementation on a CHO cell mutant is responsible for peroxisome-deficient Zellweger syndrome of complementation group I. *Proc. Natl. Acad. Sci. USA* **95**, 4350-4355. doi:10.1073/pnas.95.8.4350

Tanaka, A., Kobayashi, S. and Fujiki, Y. (2006). Peroxisome division is impaired in a CHO cell mutant with an inactivating point-mutation in dynamin-like protein 1 gene. *Exp. Cell Res.* **312**, 1671-1684. doi:10.1016/j.yexcr.2006.01.028

Touvier, T., De Palma, C., Rigamonti, E., Scagliola, A., Incerti, E., Mazelin, L., Thomas, J.-L., D'Antonio, M., Politi, L., Schaeffer, L. et al. (2015). Muscle-specific Drp1 overexpression impairs skeletal muscle growth via translational attenuation. *Cell Death Dis.* **6**, e1663. doi:10.1038/cddis.2014.595

Trompier, D., Vejux, A., Zarrouk, A., Gondcaille, C., Geillon, F., Nury, T., Savary, S. and Lizard, G. (2014). Brain peroxisomes. *Biochimie* **98**, 102-110. doi:10.1016/j.biochi.2013.09.009

Unsain, N. and Barker, P. A. (2015). New views on the misconstrued: executioner caspases and their diverse non-apoptotic roles. *Neuron* **88**, 461-474. doi:10.1016/j.neuron.2015.08.029

Veenhuis, M., Mateblowski, M., Kunau, W. H. and Harder, W. (1987). Proliferation of microbodies in Saccharomyces cerevisiae. *Yeast* **3**, 77-84. doi:10.1002/yea.320030204

Wang, C. and Youle, R. J. (2009). The role of mitochondria in apoptosis. *Annu. Rev. Genet.* **43**, 95-118. doi:10.1146/annurev-genet-102108-134850

Waterham, H. R. and Ebberink, M. S. (2012). Genetics and molecular basis of human peroxisome biogenesis disorders. *Biochim. Biophys. Acta* **1822**, 1430-1441. doi:10.1016/j.bbadis.2012.04.006

Waterham, H. R., Koster, J., van Roermund, C. W. T., Mooyer, P. A. W., Wanders, R. J. A. and Leonard, J. V. (2007). A lethal defect of mitochondrial and peroxisomal fission. *N. Engl. J. Med.* **356**, 1736-1741. doi:10.1056/NEJMoa064436

Wei, M. C., Zong, W. X., Cheng, E. H., Lindsten, T., Panoutsakopoulou, V., Ross, A. J., Roth, K. A., MacGregor, G. R., Thompson, C. B. and Korsmeyer, S. J. (2001). Proapoptotic BAX and BAK: a requisite gateway to mitochondrial dysfunction and death. *Science* **292**, 727-730. doi:10.1126/science.1059108

Weir, H. J., Yao, P., Huynh, F. K., Escoubas, C. C., Goncalves, R. L., Burkewitz, K., Laboy, R., Hirschey, M. D. and Mair, W. B. (2017). Dietary restriction and AMPK increase lifespan via mitochondrial network and peroxisome remodeling. *Cell Metab.* **26**, 884-896.e5. doi:10.1016/j.cmet.2017.09.024

Westermann, B. (2010). Mitochondrial fusion and fission in cell life and death. *Nat. Rev. Mol. Cell Biol.* **11**, 872-884. doi:10.1038/nrm3013

Wong, Y. C., Ysselstein, D. and Krainc, D. (2018). Mitochondria-lysosome contacts regulate mitochondrial fission via RAB7 GTP hydrolysis. *Nature* **554**, 382-386. doi:10.1038/nature25486

Yang, J., Liu, X., Bhalla, K., Kim, C. N., Ibrado, A. M., Cai, J., Peng, T. I., Jones, D. P. and Wang, X. (1997). Prevention of apoptosis by Bcl-2: release of cytochrome c from mitochondria blocked. *Science* **275**, 1129-1132. doi:10.1126/science.275.5303.1129

Yang, Z., Zhao, X., Xu, J., Shang, W. and Tong, C. (2018). A novel fluorescent reporter detects plastic remodeling of mitochondria-ER contact sites. *J. Cell Sci.* **131**, jcs208686. doi:10.1242/jcs.208686

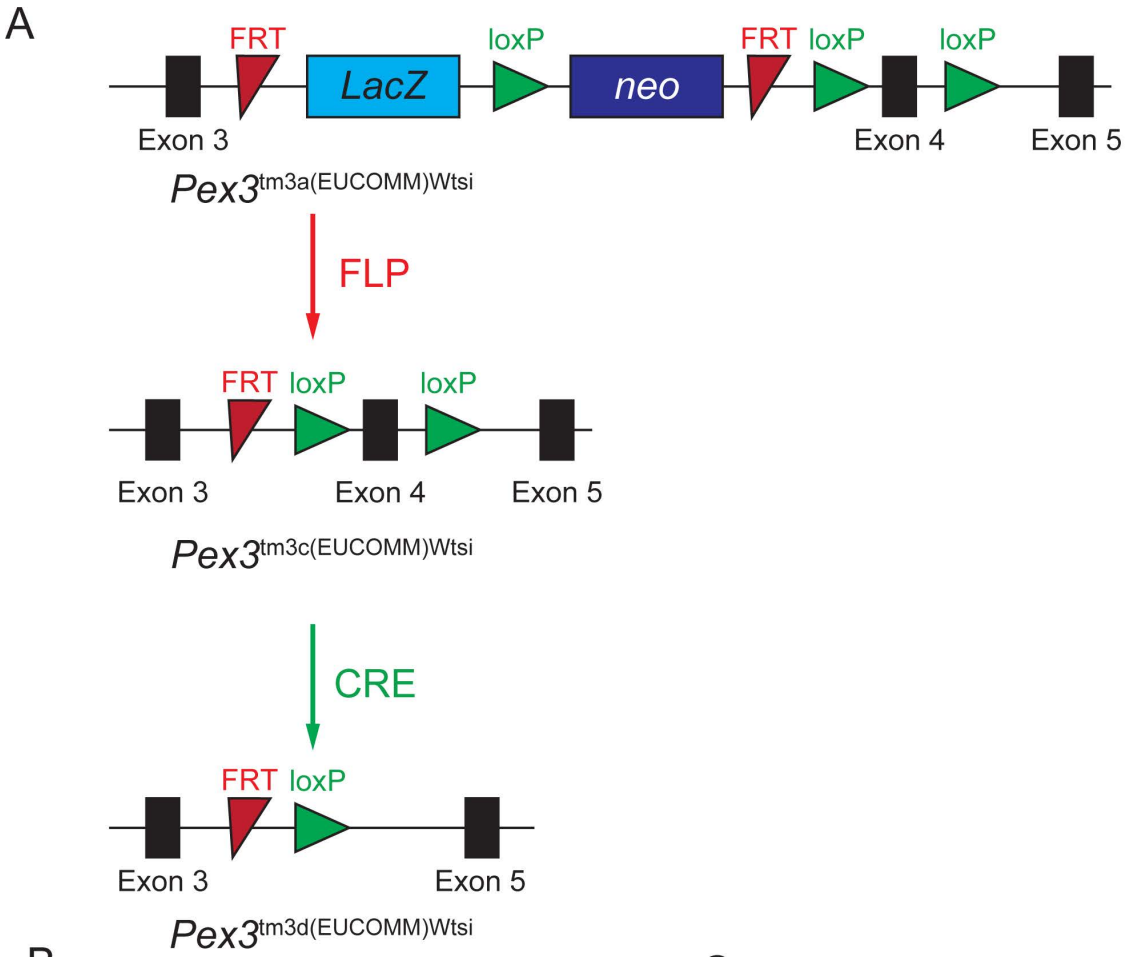

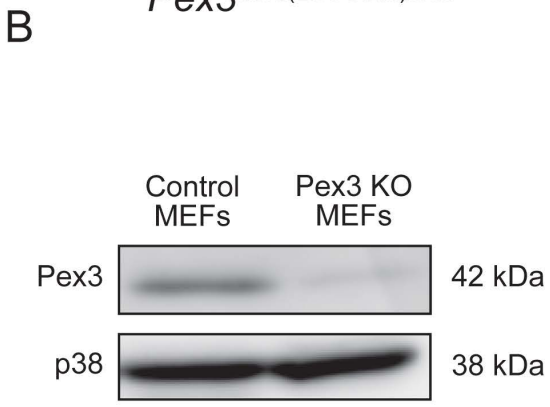

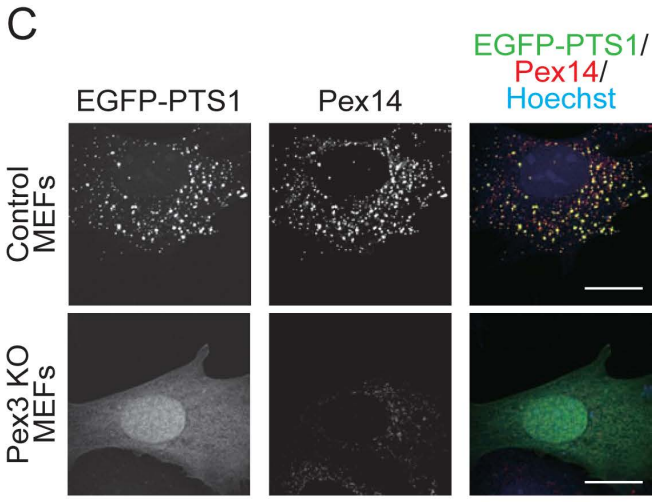

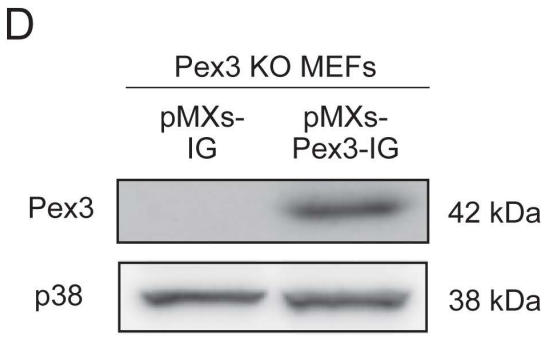

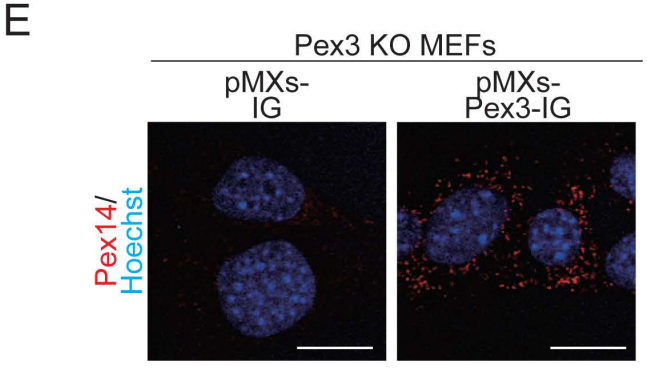

Figure S1. **Scheme for *Pex3* disruption. (A)** The region of the *Pex3* locus spanning exons 3 to 5 for *Pex3*$^{tm3a(EUCOMM)Wtsi}$, *Pex3*$^{tm3c(EUCOMM)Wtsi}$, and *Pex3*$^{tm3d(EUCOMM)Wtsi}$ alleles. See Materials and methods for details. **(B)** Immunoblot analysis of control and Pex3 KO MEFs with antibodies to Pex3 and to p38 (loading control). Data are representative of three independent experiments. **(C)** Immunofluorescence staining of control and Pex3 KO MEFs expressing EGFP-PTS1 with antibodies to Pex14. Nuclei were stained with Hoechst 33342 (1:10000). Scale bars, 20 μm. Data are representative of three independent experiments. **(D)** Immunoblot analysis of Pex3 in Pex3 KO MEFs infected with retroviruses encoding GFP either alone (pMXs-IG) or together with Pex3 (pMXs-Pex3-IG). Data are representative of three independent experiments. **(E)** Cells as in (D) were subjected to immunofluorescence staining with antibodies to Pex14. Nuclei were stained with Hoechst 33342 (1:10000). Scale bars, 20 μm. Data are representative of three independent experiments.

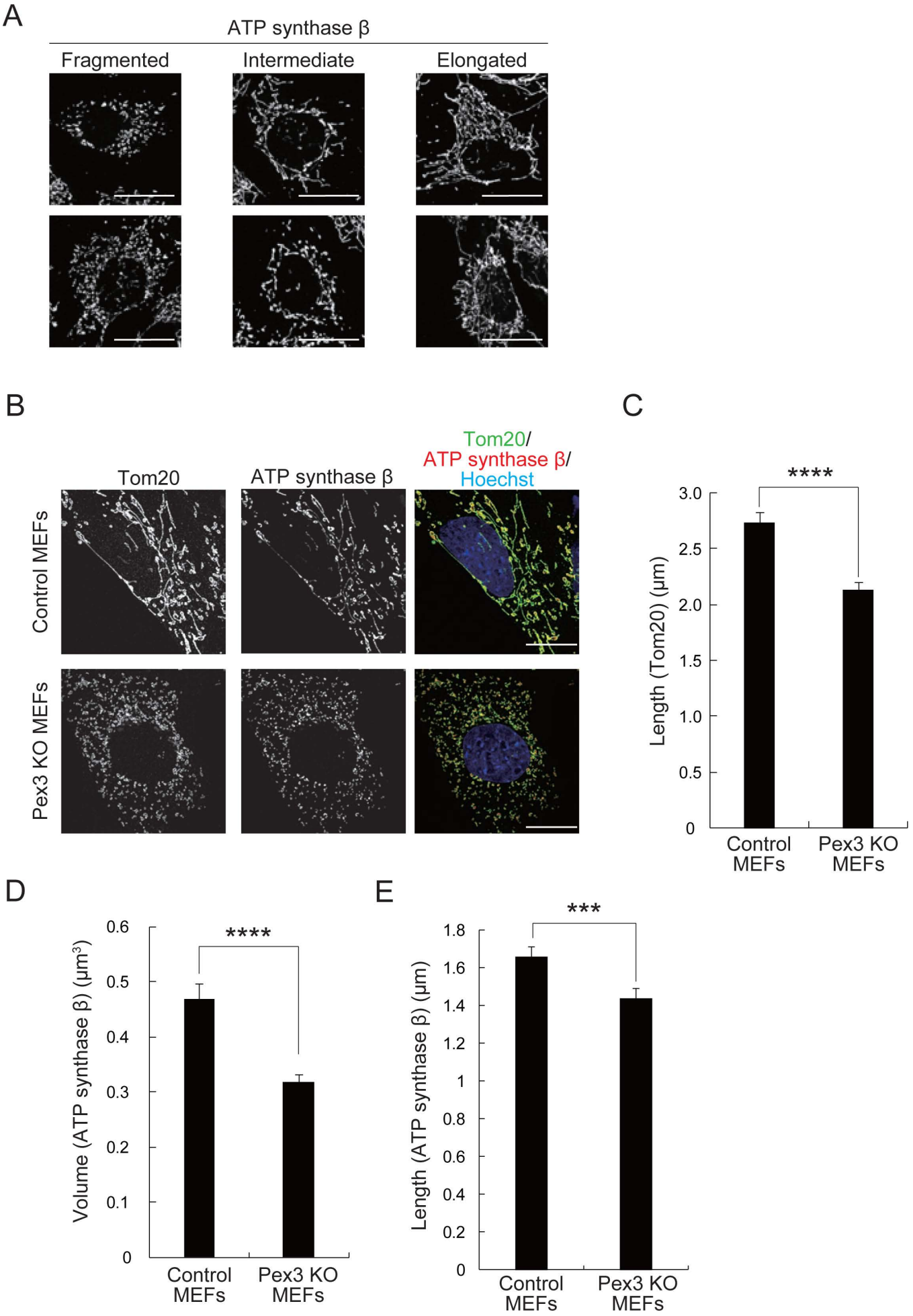

Figure S2. **Deletion of *Pex3* induces mitochondrial fragmentation.** **(A)** Representative images of "Fragmented", "Intermediate" and "Elongated" mitochondria stained with antibodies to ATP synthase β. Scale bars, 20 µm. **(B)** Deconvoluted Immunofluorescence images of control and Pex3 KO MEFs with antibodies to Tom20 and ATP synthase β. Scale bars, 20 µm. **(C)** Quantification of mitochondrial length with object analyzer, Huygens and determined from Tom20 images as in (B). Data are means ± SEM from 35 cells in control MEFs and 30 cells in Pex3 KO MEFs from three independent experiments. Threshold: 15, Seed: 50. ****P < 0.001 (unpaired Student's *t* test). **(D and E)** Quantification of mitochondrial volume and length with object analyzer, Huygens and determined from ATP synthase β images as in (B). Data are means ± SEM from 35 cells in control MEFs and 30 cells in Pex3 KO MEFs from three independent experiments. Threshold: 50, Seed:100. ***P < 0.005; ****P < 0.001 (unpaired Student's *t* test).

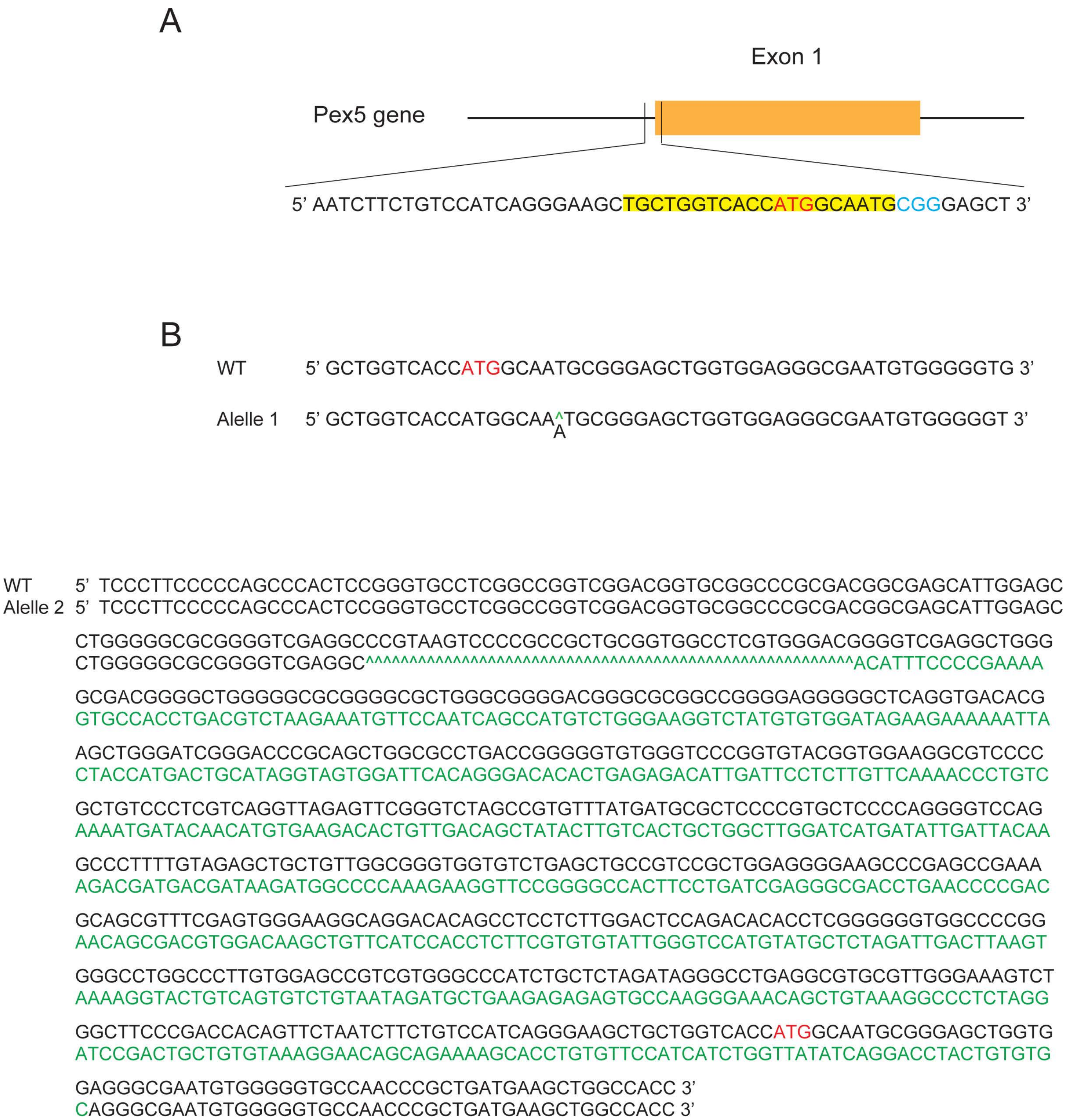

Figure S3**. Indel of *Pex5* induced with the CRISPR-Cas9 system.**

(A) Schematic representation of the targeting *Pex5* with a gRNA. The gRNA sequence is shown in yellow, protospacer adjacent motif (PAM) in blue, and start codon in red. **(B)** Sequencing of *Pex5* genomic DNA from Pex5 KO MEFs. Insertion or replacement of nucleotides is shown in green. The start codon is presented in red.

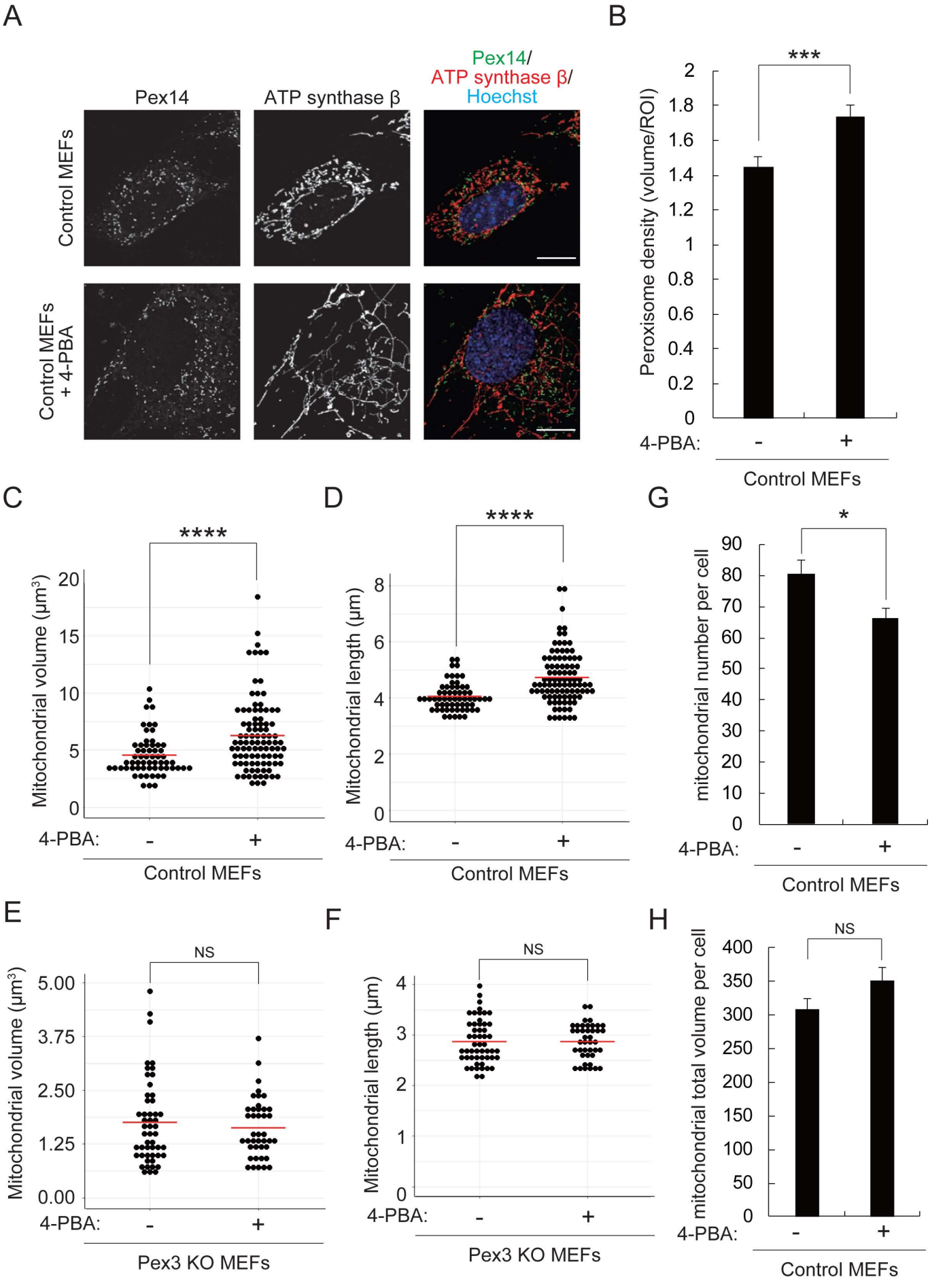

Figure S4. **The peroxisome proliferator 4-PBA induces increase of peroxisomes and mitochondrial elongation. (A)** Deconvoluted Immunofluorescence images of control MEFs with or without 1 mM 4-PBA with antibodies against Pex14 and ATP synthase β. Nuclei were stained with Hoechst 33342 (1:10000). Scale bars, 20 µm. **(B)** Quantification of peroxisome density (peroxisome volume/cell volume) with object analyzer, Huygens and determined from imaged as in (A). Data are means ± SEM from 61 cells in control MEFs and 94 cells in Control MEFs treated with 1 mM 4-PBA from four independent experiments. Threshold: 30, Seed: 60. ***P < 0.005 (unpaired Student's *t* test). **(C and D)** Quantification of mitochondrial volume and length with object analyzer, Huygens and determined from imaged as in (A). Horizontal red bars indicate means. Data are from 61 cells in control MEFs and 94 cells in control MEFs treated with 1 mM 4-PBA from four independent experiments. Threshold: 5, Seed: 30. ****P < 0.001 (unpaired Student's *t* test). **(E and F)** Quantification of mitochondrial volume and length with object analyzer, Huygens and determined from images of Pex3 KO MEFs. Horizontal red bars indicate means. Data are from 52 cells in Pex3 KO MEFs and 41 cells in Pex3 KO MEFs treated with 1 mM 4-PBA from four independent experiments. Threshold: 5, Seed: 15. NS, not significant (unpaired Student's *t* test). **(G and H)** Quantification of mitochondrial number and total volume per cell with object analyzer, Huygens and determined from imaged as in (A). Data are means ± SEM from 61 cells in control MEFs and 94 cells in control MEFs treated with 1 mM 4-PBA from four independent experiments. Threshold: 5, Seed: 30. *P < 0.05; NS, not significant (unpaired Student's *t* test).

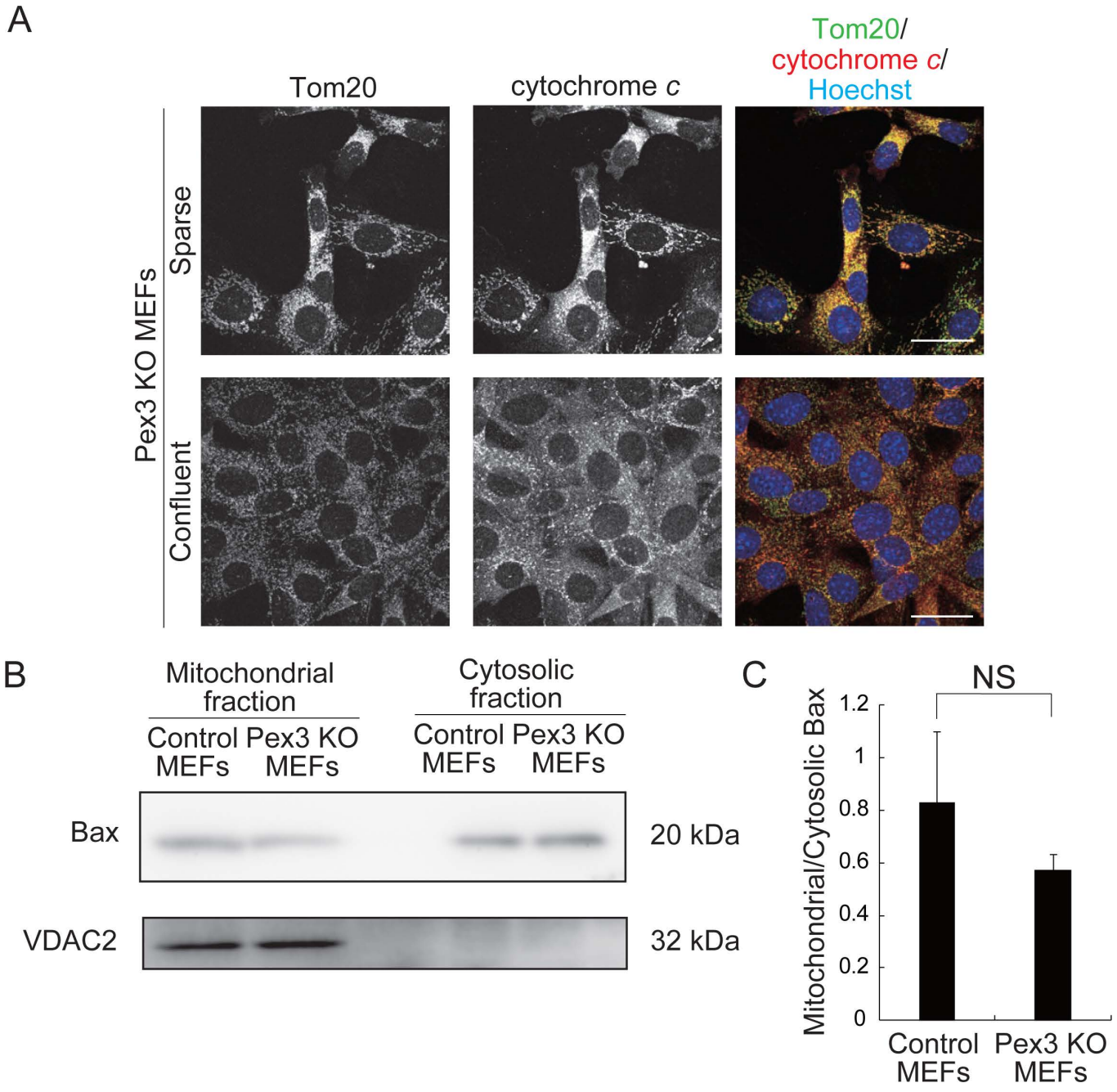

Figure S5. **A high cell density enhances cytochrome *c* diffusion of Pex3 KO MEFs. (A)** Pex3 KO MEFs seeded at low or high cell densities were subjected to immunofluorescence staining of Tom20 and cytochrome *c*. Nuclei were stained with Hoechst 33342 (1:10000). Data are representative of three independent experiments. Scale bars, 40 µm. **(B)** Subcellular fractionation analysis of Bax in control and Pex3 KO MEFs. Data are representative of three independent experiments. **(C)** Quantification of the mitochondrial/cytosolic Bax in blots similar to those in (B). Data are means ± SEM for three independent experiments. NS, not significant (paired Student's *t* test).

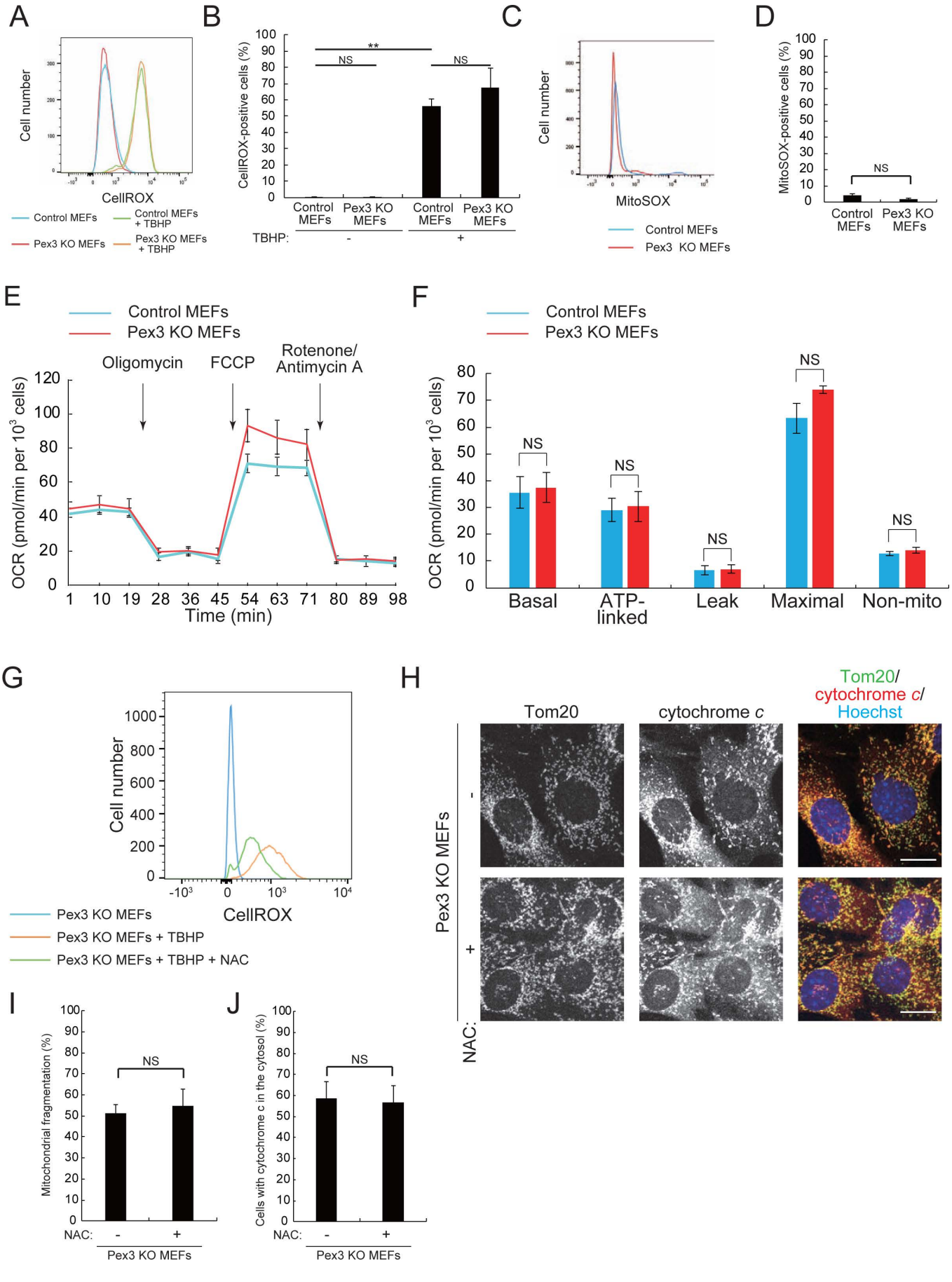

Figure S6. ***Pex3* deletion without overt changes in ROS and respiration levels. (A)** Representative flow cytometric analysis of cytosolic ROS levels as detected by CellROX staining in control and Pex3 KO MEFs incubated with or without 200 μM TBHP for 60 minutes. **(B)** Quantification of CellROX-positive cells as in (A). Data are means ± SEM from three independent experiments. **P < 0.01; NS, not significant (Scheffe's test). **(C)** Representative flow cytometric analysis of mitochondrial ROS levels as detected by MitoSOX staining in control and Pex3 KO MEFs. **(D)** Quantification of MitoSOX-positive cells as in (C). Data are means ± SEM from six independent experiments. NS, not significant (paired Student's *t* test). **(E)** Oxygen consumption rate (OCR) in control and Pex3 KO MEFs. Data are means ± SEM of triplicates from a representative experiment. **(F)** Basal, ATP-linked, proton-leak (+oligomycin), maximal (+CCCP), and nonmitochondrial (Non-mito, +rotenone/antimycin A) OCR determined as in (E). Data are means ± SEM from three independent experiments. NS, not significant (unpaired Student's *t* test). **(G)** Flow cytometric analysis of cytosolic ROS as detected by CellROX staining in Pex3 KO MEFs incubated with or without 5 mM NAC for 1 hour and then in the additional absence or presence of 200 μM TBHP for 1 hour. Data are representative of three independent experiments. **(H)** Immunofluorescence staining of Tom20 and cytochrome *c* in Pex3 KO MEFs incubated with or without 5 mM NAC for 6 hours. Nuclei were also stained with Hoechst 33342 (1:10000). Scale bars, 20 μm. **(I and J)** Quantification of mitochondrial fragmentation and the diffusion of cytochrome *c* into the cytosol, respectively, for images similar to those in (H). Data are means ± SEM for three independent experiments. NS, not significant (unpaired Student's *t* test).

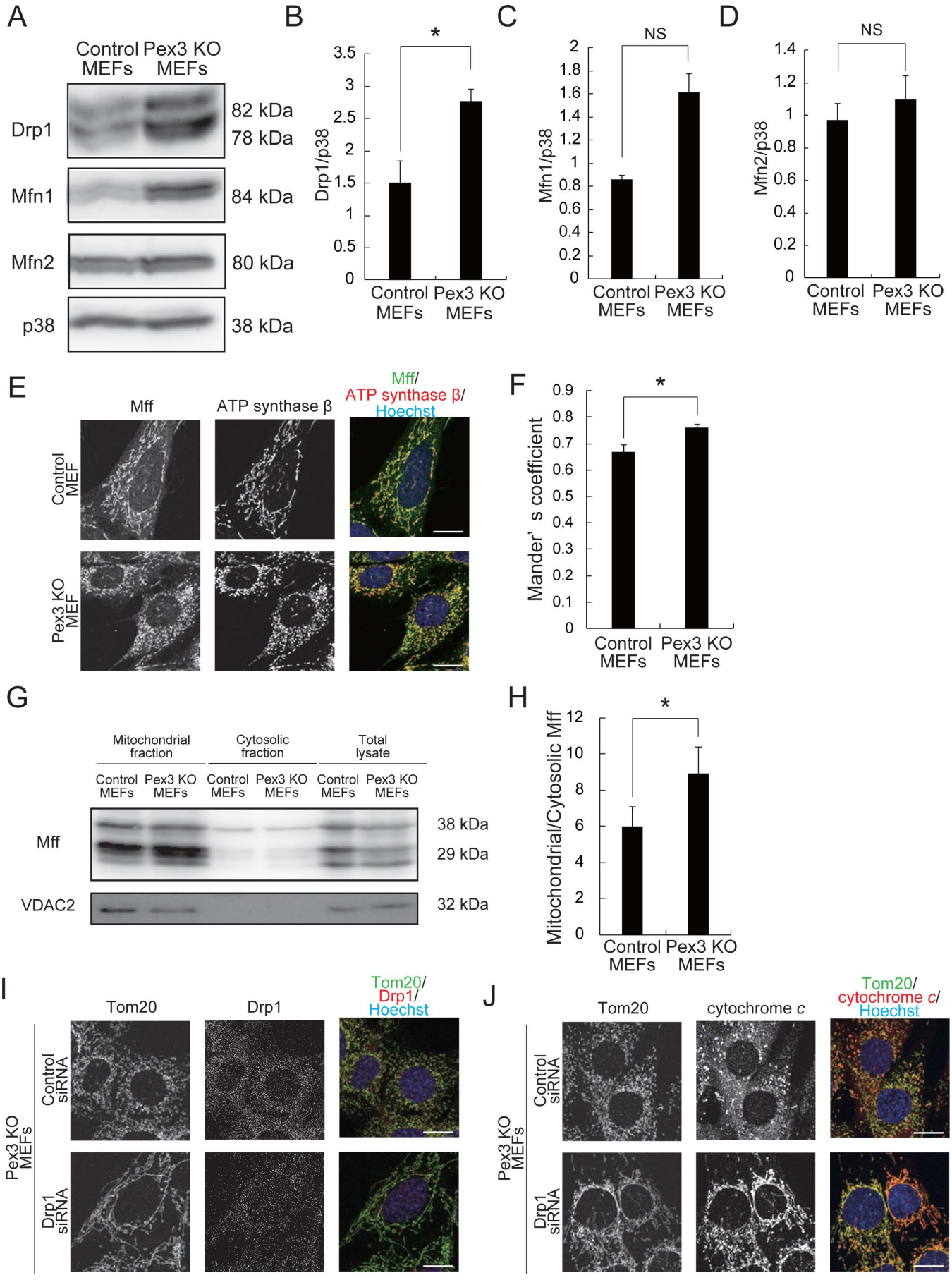

Figure S7. **Drp1 contributes to mitochondrial fragmentation and cytochrome c diffusion in Pex3 KO MEFs. (A)** Immunoblot analysis of Drp1, Mfn1 and Mfn2 in control and Pex3 KO MEFs. **(B-D)** Quantification of Drp1, Mfn1 and Mfn2 (normalized by p38) in blots similar to those in (A). Data are means ± SEM for three independent experiments. *P < 0.05; NS, not significant (paired Student's *t* test). **(E)** Immunofluorescence staining of Mff and ATP synthase β in control and Pex3 KO MEFs. Nuclei were stained with Hoechst 33342 (1:10000). Scale bars, 20 μm. Data are representative of three independent experiments. **(F)** Colocalization of Mff with ATP synthase β as reflected by Manders' M2 coefficient and determined from images as in (E). Data are means ± SEM for three independent experiments. *P < 0.05 (unpaired Student's *t* test). **(G)** Subcellular fractionation analysis of Mff in control and Pex3 KO MEFs. Data are representative of four independent experiments. **(H)** Quantification of the mitochondrial/cytosolic Mff in blots similar to those in (G). Data are means ± SEM for four independent experiments. *P < 0.05 (paired Student's *t* test). **(I)** Immunofluorescence staining of Tom20 and Drp1 in Pex3 KO MEFs transfected with siRNA targeting Drp1 or control siRNA. Nuclei were stained with Hoechst 33342 (1:10000). Scale bars, 20 μm. Data are representative of three independent experiments. **(J)** Immunofluorescence staining of Tom20 and cytochrome *c* in Pex3 KO MEFs transfected with siRNA targeting Drp1 or control siRNA. Nuclei were stained with Hoechst 33342 (1:10000). Scale bars, 20 μm. Data are representative of three independent experiments.

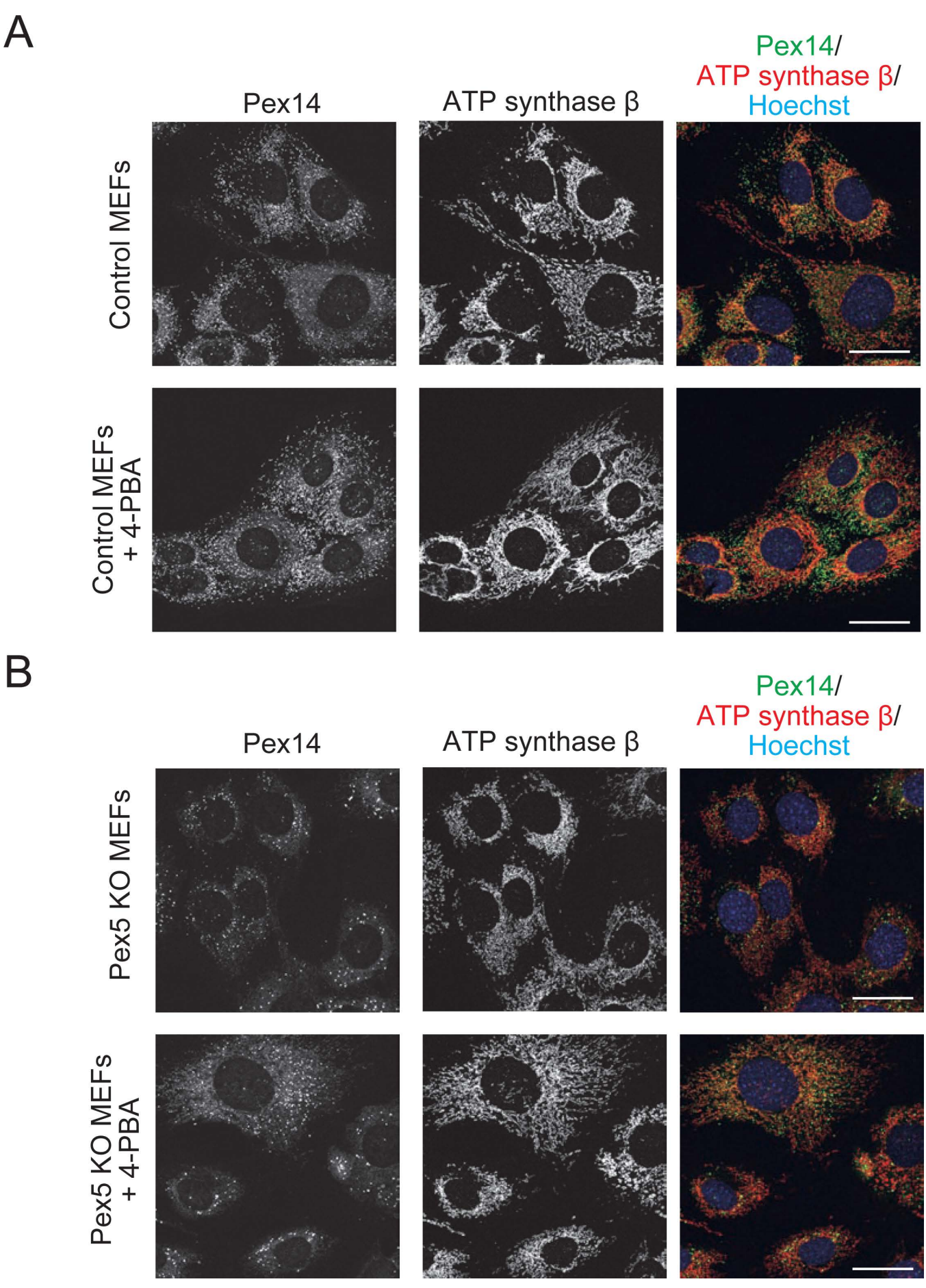

Figure S8. **Peroxisome proliferator 4-PBA increases the amount of peroxisomes and elongates mitochondria in a fraction of Pex5 KO MEFs.** **(A)** Immunofluorescence staining of Pex14 and ATP synthase β (mitochondrial marker) in control MEFs cultured with or without 5 mM 4-PBA for 48 hours. Nuclei were stained with Hoechst 33342. Scale bars, 40 μm. **(B)** Immunofluorescence staining of Pex14 and ATP synthase β in Pex5 KO MEFs cultured with or without 5 mM 4-PBA for 48 hours. Nuclei were stained with Hoechst 33342 (1:10000). Scale bars, 40 μm. Data are representative of three independent experiments.